

RECEIVED: April 5, 2023

REVISED: October 23, 2023

ACCEPTED: January 15, 2024

PUBLISHED: January 25, 2024

Study of new physics effects in $\bar{B}_s \rightarrow D_s^{(*)} \tau^- \bar{\nu}_\tau$ semileptonic decays using lattice QCD form factors and heavy quark effective theory

Neus Penalva ^a, Jonathan M. Flynn ^b, Eliecer Hernández ^c and Juan Nieves ^a

^a*Instituto de Física Corpuscular (centro mixto CSIC-UV), Institutos de Investigación de Paterna, C/Catedrático José Beltrán 2, E-46980 Paterna, Valencia, Spain*

^b*Physics & Astronomy, University of Southampton, Southampton SO17 1BJ, U.K.*

^c*Departamento de Física Fundamental e IUFFyM, Universidad de Salamanca, Plaza de la Merced s/n, E-37008 Salamanca, Spain*

E-mail: neus.penalva@icc.uv.es, j.m.flynn@soton.ac.uk, gajateee@usal.es, jmnieves@ific.uv.es

ABSTRACT: We benefit from the lattice QCD determination by the HPQCD of the Standard Model (SM) form factors for the $\bar{B}_s \rightarrow D_s$ [*Phys. Rev. D* **101** (2020) 074513] and the SM and tensor ones for the $\bar{B}_s \rightarrow D_s^*$ ([arXiv:2304.03137](https://arxiv.org/abs/2304.03137) [hep-lat]) semileptonic decays, and the heavy quark effective theory (HQET) relations for the analogous $B \rightarrow D^{(*)}$ decays obtained by F.U. Bernlochner et al. in *Phys. Rev. D* **95** (2017) 115008, to extract the leading and sub-leading Isgur-Wise functions for the $\bar{B}_s \rightarrow D_s^{(*)}$ decays. Further use of the HQET relations allows us to evaluate the corresponding scalar, pseudoscalar and tensor form factors needed for a phenomenological study of new physics (NP) effects on the $\bar{B}_s \rightarrow D_s^{(*)}$ semileptonic decay. At present, the experimental values for the ratios $\mathcal{R}_{D^{(*)}} = \Gamma[\bar{B} \rightarrow D^{(*)} \tau^- \bar{\nu}_\tau] / \Gamma[\bar{B} \rightarrow D^{(*)} e^- (\mu^-) \bar{\nu}_{e(\mu)}]$ are the best signal in favor of lepton flavor universality violation (LFUV) seen in charged current (CC) $b \rightarrow c$ decays. In this work we conduct a study of NP effects on the $\bar{B}_s \rightarrow D_s^{(*)} \tau^- \bar{\nu}_\tau$ semileptonic decays by comparing tau spin, angular and spin-angular asymmetry distributions obtained within the SM and three different NP scenarios. As expected from SU(3) light-flavor symmetry, we get results close to the ones found in a similar analysis of the $\bar{B} \rightarrow D^{(*)}$ case. The measurement of the $\bar{B}_s \rightarrow D_s^{(*)} \ell \bar{\nu}_\ell$ semileptonic decays, which is within reach of present experiments, could then be of relevance in helping to establish or rule out LFUV in CC $b \rightarrow c$ transitions.

KEYWORDS: Effective Field Theories of QCD, Flavour Symmetries, Semi-Leptonic Decays, SMEFT

ARXIV EPRINT: [2304.00250](https://arxiv.org/abs/2304.00250)

Contents

1	Introduction	1
2	HQET fit of the $\bar{B}_s \rightarrow D_s^{(*)}$ semileptonic-decay LQCD form factors and SM distributions	3
2.1	LQCD form factors	4
2.1.1	$\bar{B}_s \rightarrow D_s$	4
2.1.2	$B_s \rightarrow D_s^*$	5
2.2	HQSS form factors	6
2.3	Fit of the SM-LQCD form factors to their HQSS/HQET expressions.	8
2.4	Visible kinematics of the sequential $H_b \rightarrow H_c \tau^- (\pi^- \nu_\tau, \rho^- \nu_\tau, \ell^- \bar{\nu}_\ell \nu_\tau) \bar{\nu}_\tau$ decays	10
3	New physics effects in $\bar{B}_s \rightarrow D_s^{(*)} \tau^- \nu_\tau$ semileptonic decays	14
3.1	$H_b \rightarrow H_c \ell^- \bar{\nu}_\ell$ Effective Hamiltonian	15
3.2	Partially integrated sequential $H_b \rightarrow H_c \tau^- (\pi^- \nu_\tau, \rho^- \nu_\tau, \ell^- \bar{\nu}_\ell \nu_\tau) \bar{\nu}_\tau$ decay distributions	16
3.3	NP results and discussion	17
3.3.1	LFUV ratios, unpolarized differential decay widths and tau angular, spin and spin-angular asymmetries	17
3.3.2	Distributions of charged tau decay products	20
4	Summary	24
A	Mean values and covariance matrices of the a_i^F coefficients in eqs. (2.6), (2.7) and (2.9)	25

1 Introduction

Present experimental data on $\bar{B} \rightarrow D^{(*)}$ semileptonic decays points to the possibility of lepton flavor universality violation (LFUV) that will affect charged-current (CC) $b \rightarrow c \tau^- \bar{\nu}_\tau$ semileptonic transitions. The ratios $\mathcal{R}_D = \Gamma(\bar{B} \rightarrow D \tau^- \bar{\nu}_\tau) / \Gamma(\bar{B} \rightarrow D \mu^- \bar{\nu}_\mu)$ and $\mathcal{R}_{D^*} = \Gamma(\bar{B} \rightarrow D^* \tau^- \bar{\nu}_\tau) / \Gamma(\bar{B} \rightarrow D^* \mu^- \bar{\nu}_\mu)$ have been measured by the BaBar [1, 2], Belle [3–6] and LHCb [7–10] experiments and their combined analysis by the HFLAV collaboration indicates a 3σ tension with SM predictions [11, 12].

LFUV requires the existence of new physics (NP) beyond the Standard Model (SM) and, if confirmed, would have a tremendous impact in particle physics. This makes the study of as many analogous CC decays as possible timely and necessary in order to confirm or rule out LFUV. The $\mathcal{R}_{J/\psi} = \Gamma(\bar{B}_c \rightarrow J/\psi \tau^- \bar{\nu}_\tau) / \Gamma(\bar{B}_c \rightarrow J/\psi \mu^- \bar{\nu}_\mu)$ ratio has been measured by the LHCb collaboration [13] finding a 1.8σ discrepancy with SM results [14–26]. Another reaction where a similar behavior was to be expected is the baryon $\Lambda_b \rightarrow \Lambda_c \ell \bar{\nu}_\ell$ decay. However, in this case, the recent measurement of the $\mathcal{R}_{\Lambda_c} = \Gamma(\Lambda_b \rightarrow \Lambda_c \tau^- \bar{\nu}_\tau) / \Gamma(\Lambda_b \rightarrow \Lambda_c \mu^- \bar{\nu}_\mu)$ ratio by the

LHCb collaboration [27] is in agreement, within errors, with the SM prediction [28]. In this experiment, the τ^- lepton was reconstructed using the $\tau^- \rightarrow \pi^- \pi^+ \pi^- (\pi^0) \nu_\tau$ hadronic decay. It is then of great interest to see whether the current \mathcal{R}_{Λ_c} experimental value is confirmed or not using the muonic reconstruction channel. Such an analysis is under way [29].

LHCb has very recently [10] presented the first simultaneous measurement in hadron collisions of \mathcal{R}_{D^*} and \mathcal{R}_{D^0} , identifying the tau lepton from its the decay mode $\tau^- \rightarrow \mu^- \nu_\tau \bar{\nu}_\mu$. The measured values are $\mathcal{R}_{D^*} = 0.281 \pm 0.018 \pm 0.024$ and $\mathcal{R}_{D^0} = 0.441 \pm 0.060 \pm 0.066$, where the correlation between these measurements is -0.43 . The result for the former ratio supersedes the higher value previously reported in [7] and it is now in better agreement with the SM. LHCb earlier measured $\mathcal{R}_{D^*} = 0.291 \pm 0.019 \pm 0.026 \pm 0.013$ [8, 9] using hadronic tau decays, but a new result was reported in [30], $\mathcal{R}_{D^*} = 0.257 \pm 0.012 \pm 0.014 \pm 0.012$, obtained after combining the previous results from refs. [8, 9] and a new one from a partial Run 2 data sample [30]. The final LHCb result for \mathcal{R}_{D^*} from hadronic tau decays is in closer agreement with the SM expectation. Nevertheless combined global results for \mathcal{R}_{D^*} and \mathcal{R}_D from different experiments and detection techniques remain around 3σ away from the SM expectation (HFLAV Winter 2023 update [31] presented in [12]).

One would also expect to see LFUV effects in $\bar{B}_s \rightarrow D_s^{(*)}$ semileptonic decays which are SU(3) analogues of the $\bar{B} \rightarrow D^{(*)}$ ones. A measurement of \mathcal{R}_{D_s} by LHCb [12] is also underway, making the study of these reactions timely. The theoretical analysis of NP effects in those decays requires however knowledge of beyond-the-SM (BSM) form factors that have not yet been determined. The HPQCD lattice QCD (LQCD) collaboration has evaluated the SM form factors for the $\bar{B}_s \rightarrow D_s$ and $\bar{B}_s \rightarrow D_s^*$ semileptonic transitions in refs. [32] and [33], respectively. More recently, HPQCD has given updated $\bar{B}_s \rightarrow D_s^*$ SM form-factors [34]. This latter work also provides the form factors that expand the matrix elements of the NP $\bar{c}\sigma^{\mu\nu}b$ operator for initial \bar{B}_s and final D_s^* states.

On the other hand, the approximate heavy quark spin symmetry (HQSS) of QCD allows one to construct an effective field theory (HQET) to compute these form-factors. Indeed, the HQET expressions for them can be obtained up to next-to-leading (NLO) $\mathcal{O}(\alpha_s, \Lambda_{\text{QCD}}/m_{c,b})$ and next-to-next-to-leading (NNLO) $\mathcal{O}(\alpha_s \Lambda_{\text{QCD}}/m_{c,b}, \Lambda_{\text{QCD}}^2/m_{c,b}^2)$ orders from refs. [35] and [36], respectively.¹ One can use this information to fit the leading and sub-leading HQSS Isgur-Wise (IW) functions, which describe the $\bar{B}_s \rightarrow D_s^{(*)}$ form factors, to the lattice data of refs. [32] and [34]. First, from the comparison of results to those available for $\bar{B} \rightarrow D^{(*)}$ decays, one could in principle estimate the size of the SU(3) light-flavor breaking corrections. Second, and more interesting, once the IW functions are known, the scalar, pseudoscalar and tensor² form factors that are needed, in addition to the SM ones, for an analysis of possible NP effects on the $\bar{B}_s \rightarrow D_s^{(*)} \tau \bar{\nu}_\tau$ decays can be obtained from their HQET expressions. Thus, we will show results for tau spin, angular and spin-angular asymmetry distributions for these decays obtained within the SM and three different NP scenarios, and analyze the role that different tau asymmetries in the $\bar{B}_s \rightarrow D_s^{(*)} \tau \bar{\nu}_\tau$ decay could play, not only in establishing the existence of NP, but also in distinguishing between different NP extensions of the SM. We

¹The partial NNLO $\mathcal{O}(\Lambda_{\text{QCD}}^2/m_c^2)$ corrections were previously studied in refs. [37, 38].

²As already mentioned, LQCD tensor form factors were computed in [34] for the $\bar{B}_s \rightarrow D_s^*$ transition. However, there is no LQCD input on the tensor matrix element in the case of the $\bar{B}_s \rightarrow D_s$ decay mode.

will also study partially integrated angular and energy distributions of the charged particle produced in the subsequent $\tau^- \rightarrow \pi^- \nu_\tau, \rho^- \nu_\tau, e^- (\mu^-) \bar{\nu}_{e(\mu)} \nu_\tau$ decays. The latter differential decay widths have a better statistics than the asymmetries themselves and they could also help in establishing the presence of NP beyond the SM.

The $\bar{B}_s \rightarrow D_s^{(*)}$ form-factors have also been studied using HQET and sum rules in [38]. In that work, additional constraints are found which allow the authors to go beyond the assumption of SU(3) flavor symmetry, and SM lepton-flavour universality ratios are reported. NP effects on both $\bar{B}_s \rightarrow D_s$ and $\bar{B}_s \rightarrow D_s^*$ decays have been discussed in [39, 40] using the SM LQCD form-factors computed in refs. [41] and [33], respectively. The works of refs. [39, 40] do not consider NP tensor operators and make use of the equations of motion to estimate the NP scalar and pseudo-scalar form-factors. The distribution of the tau-decay products is not studied in either of the two works and hence they do not have access to the full set of tau angular, tau spin and tau angular-spin asymmetries that can be extracted by measuring the τ in a general polarization state. Moreover those papers do not address the distribution of the tau-decay products. However, different angular distributions from the decay products of the outgoing D_s^* are studied in [40].

In ref. [36], the NNLO corrections were computed introducing (postulating) a supplemental power counting within HQET. The authors of that work claimed that the postulated truncation leads to small, highly constrained set of second-order power corrections, compared to the standard approach. Nevertheless, there appears a plethora of free parameters, a number considerably larger than in the NLO case of ref. [35]. Though, it seems the scheme followed in ref. [36] provides excellent fits to the available $\bar{B} \rightarrow D^{(*)}$ LQCD predictions and experimental data, we have found that the NNLO parameters cannot be determined reliably from the available $\bar{B}_s \rightarrow D_s$ and $\bar{B}_s \rightarrow D_s^*$ LQCD form-factor data, given the statistical and systematic precision with which they are currently obtained. For that reason, we will limit this work to NLO HQET corrections, except in the case of the form factors that are protected from $\mathcal{O}(\Lambda_{\text{QCD}}^2/m_c)$ corrections at zero recoil [42], for which we will include NNLO $\mathcal{O}[\Lambda_{\text{QCD}}^2/m_c^2]$ terms. These form factors do not vanish in the heavy quark limit and turn out to be the best determined in the LQCD simulations, in particular near zero recoil, making it necessary to consider some sub-leading corrections in addition to those induced by short-distance physics.

This work is organized as follows. In section 2 we describe the fitting procedure to obtain the IW functions, with some auxiliary details collected in the appendix. A thorough analysis of NP effects, based on observables that can be measured by the analysis of the visible kinematics of the subsequent hadronic $\tau^- \rightarrow \pi^- \nu_\tau, \tau^- \rightarrow \rho^- \nu_\tau$ and leptonic $\tau^- \rightarrow \ell^- \bar{\nu}_\ell \nu_\tau$ decays, is conducted in section 3. Finally in section 4 we summarize the main findings.

2 HQET fit of the $\bar{B}_s \rightarrow D_s^{(*)}$ semileptonic-decay LQCD form factors and SM distributions

In this section we will describe how we fit the LQCD form-factor data from refs. [32, 34] to their expressions deduced from NLO HQET and derived in ref. [35]. A comparison of both sets of form factors will be shown below in figure 3. We will also show the SM predictions from both sets for differential decay widths and tau spin, angular and spin-angular asymmetry distributions. Further use of HQSS will allow us to predict BSM form factors not evaluated

in the lattice, and that are needed to test possible NP effects in $\bar{B}_s \rightarrow D_s^{(*)} \tau^- \bar{\nu}_\tau$ semileptonic decays, something we will do in the next section.

2.1 LQCD form factors

We will use the LQCD results from HPQCD for the SM form factors of the $\bar{B}_s \rightarrow D_s$ decay [32] and the SM and tensor form factors of the $\bar{B}_s \rightarrow D_s^*$ decay [34].

2.1.1 $\bar{B}_s \rightarrow D_s$

For the $\bar{B}_s \rightarrow D_s$ semileptonic decay, the form-factor decomposition in ref. [32] is

$$\langle D_s; \vec{p}' | \bar{c}(0) \gamma^\mu b(0) | \bar{B}_s; \vec{p} \rangle = f_+(q^2) \left[p^\mu + p'^\mu - \frac{M_{\bar{B}_s}^2 - M_{D_s}^2}{q^2} q^\mu \right] + f_0(q^2) \frac{M_{\bar{B}_s}^2 - M_{D_s}^2}{q^2} q^\mu, \quad (2.1)$$

with the constraint

$$f_0(0) = f_+(0). \quad (2.2)$$

The form factors are parametrized as [32]

$$\begin{aligned} f_0(q^2) &= \frac{1}{1 - q^2/M_{B_c0}^2} \sum_{n=0}^2 \tilde{a}_n^0 z^n, \\ f_+(q^2) &= \frac{1}{1 - q^2/M_{B_c^*}^2} \sum_{n=0}^2 \tilde{a}_n^+ \left[z^n - \frac{(-1)^{n-3} n}{3} z^3 \right], \end{aligned} \quad (2.3)$$

where q^μ is the four-momentum transfer to the leptons and

$$\tilde{z}(q^2) = z(q^2; t_{\text{th}}, 0), \quad t_{\text{th}} = (M_{B_s} + M_{D_s})^2. \quad (2.4)$$

where

$$z(q^2; t_{\text{th}}, t_0) = \frac{\sqrt{t_{\text{th}} - q^2} - \sqrt{t_{\text{th}} - t_0}}{\sqrt{t_{\text{th}} - q^2} + \sqrt{t_{\text{th}} - t_0}}, \quad (2.5)$$

The constraint in eq. (2.2) imposes $\tilde{a}_0^0 = \tilde{a}_0^+$.

To improve the quality of our HQSS form-factor fit, we change the parametrization above and symmetrize the range of z corresponding to $0 \leq q^2 \leq t_-$ where $t_- = (M_{B_s} - M_{D_s})^2$. Thus, we use

$$f_0(q^2) = \frac{1}{1 - q^2/M_{B_c0}^2} \sum_{n=0}^2 a_n^0 z^n, \quad f_+(q^2) = \frac{1}{1 - q^2/M_{B_c^*}^2} \sum_{n=0}^2 a_n^+ z^n, \quad (2.6)$$

with

$$z(q^2) = z(q^2; t_{\text{th}}, t_0), \quad t_{\text{th}} = (M_B + M_D)^2, \quad t_0 = t_{\text{th}} - \sqrt{t_{\text{th}}(t_{\text{th}} - t_-)}. \quad (2.7)$$

The central values and errors of the new expansion coefficients, together with the corresponding correlation matrix, are collected in table 6 of the appendix. Note that we use eq. (2.2) to fix a_2^+ for $\bar{B}_s \rightarrow D_s$. The quality of this new expansion can be seen in figure 1 where we compare the new parameterization with the original one in ref. [32]. The agreement is excellent.

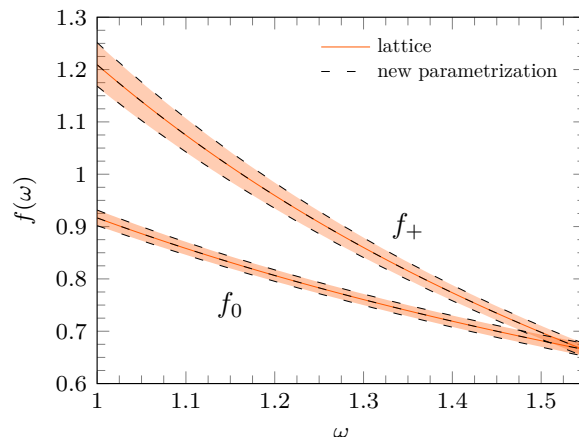


Figure 1. Comparison of the original SM-LQCD form factors for $\bar{B}_s \rightarrow D_s$ [32] and their description in this work using the parametrization of eq. (2.6). Both central values and 68% confidence level (CL) bands show excellent agreement.

2.1.2 $B_s \rightarrow D_s^*$

In this case, in ref. [34] they use the HQET basis to expand the matrix elements of the vector, axial and tensor quark-current operators

$$\begin{aligned}
 \langle D_s^*; \vec{p}', r | \bar{c}(0) \gamma^\mu b(0) | \bar{B}_s; \vec{p} \rangle &= i \sqrt{M_{B_s} M_{D_s^*}} h_V(q^2) \epsilon^{\mu\nu\rho\sigma} \epsilon_\nu^*(\vec{p}', r) v'_\rho v_\sigma, \\
 \langle D_s^*; \vec{p}', r | \bar{c}(0) \gamma^\mu \gamma_5 b(0) | \bar{B}_s; \vec{p} \rangle &= \sqrt{M_{B_s} M_{D_s^*}} \{ h_{A_1}(q^2) (\omega + 1) \epsilon^{*\mu}(\vec{p}', r) - h_{A_2}(q^2) [\epsilon^{*\mu}(\vec{p}', r) \cdot v] v^\mu \\
 &\quad - h_{A_3}(q^2) [\epsilon^{*\mu}(\vec{p}', r) \cdot v] v'^\mu \} \\
 \langle D_s^*; \vec{p}', r | \bar{c}(0) \sigma^{\mu\nu} b(0) | \bar{B}_s; \vec{p} \rangle &= -\sqrt{M_{B_s} M_{D_s^*}} \{ h_{T_1}(q^2) \epsilon_\alpha^*(\vec{p}', r) (v + v')_\beta \\
 &\quad + h_{T_2}(q^2) \epsilon_\alpha^*(\vec{p}', r) (v - v')_\beta + h_{T_3}(q^2) [\epsilon^*(\vec{p}', r) \cdot v] v_\alpha v'_\beta \} \epsilon^{\mu\nu\alpha\beta},
 \end{aligned} \tag{2.8}$$

where $\epsilon^*(\vec{p}', r)$ is the polarization vector of the final D_s^* meson, $v(v')$ is the four-velocity of the $\bar{B}_c(D_s^*)$ meson and $\omega = v \cdot v'$. The convention $\epsilon_{0123} = +1$ is used.

In ref. [34], the above form factors include a third-degree polynomial in $\omega - 1$, logarithms determined from staggered chiral perturbation theory and some extra analytical dependence on $M_{\pi(K)}^2$. The continuum-limit values can be extracted from the supplemental material available in the source file provided in ref. [34]. Since the logarithms have a very mild dependence on $\omega - 1$, and in order to facilitate the further HQSS form-factor fit that we are going to conduct, we have made a description of the lattice form factors just as a third-degree polynomial in $\omega - 1$. Thus, we use

$$h_F(\omega) = \sum_{n=0}^3 a_n^F (\omega - 1)^n. \tag{2.9}$$

In the appendix, we give the central values and errors of the new expansion coefficients in tables 7 and 8 while the correlation matrix is compiled in tables 9 to 13. Again, the quality of these new expansions can be seen in figure 2, where we compare the results of the

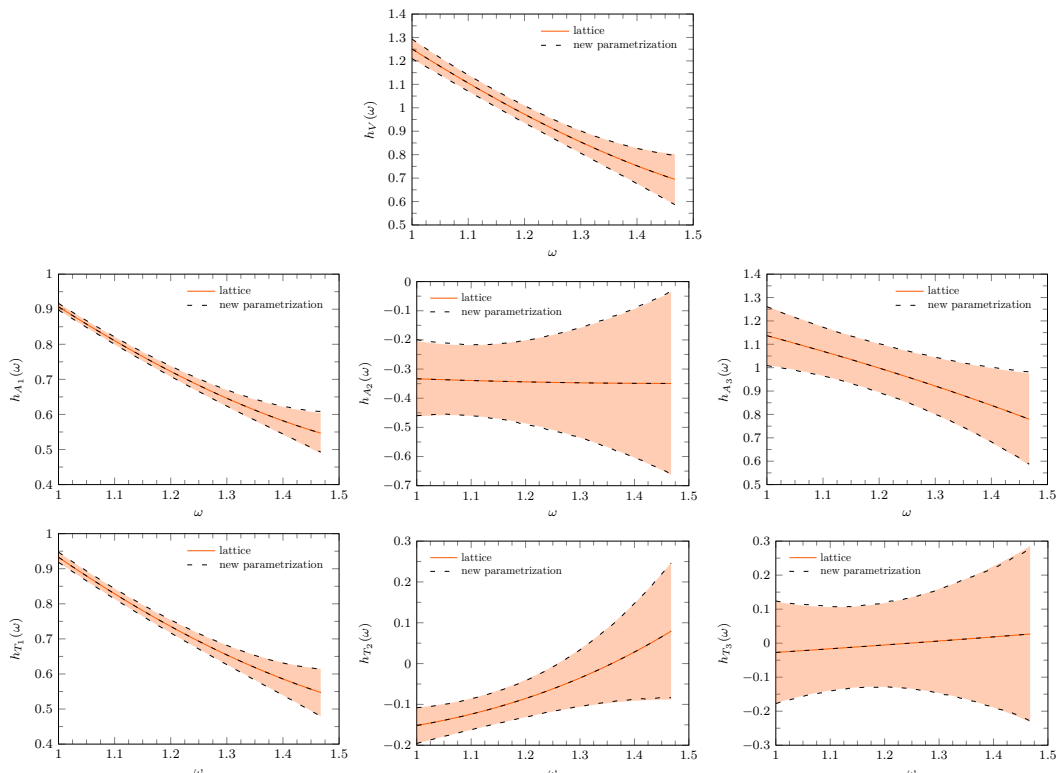


Figure 2. Comparison of the original LQCD form factors for $\bar{B}_s \rightarrow D_s^*$ [34] and their description in this work using the parametrization of eq. (2.9). Both central values and 68% confidence level (CL) bands show excellent agreement.

simpler parametrization in eq. 2.9 with the original lattice values in ref. [32]. The agreement is once again excellent.

2.2 HQSS form factors

In HQET, for $\bar{B}_s \rightarrow D_s$, one normally uses the following form-factor decomposition of the transition-current matrix elements [35]

$$\langle D_s; \vec{p}' | \bar{c}(0) \gamma^\mu b(0) | \bar{B}_s; \vec{p} \rangle = \sqrt{M_{B_s} M_{D_s}} [h_+(\omega)(v^\mu + v'^\mu) + h_-(\omega)(v^\mu - v'^\mu)], \quad (2.10)$$

with h_\pm related to f_+ and f_0 above through

$$\begin{aligned} f_+ &= \frac{1}{2\sqrt{M_{B_s} M_{D_s}}} [(M_{B_s} + M_{D_s}) h_+ - (M_{B_s} - M_{D_s}) h_-] \\ f_0 &= \sqrt{M_{B_s} M_{D_s}} \left[\frac{\omega + 1}{M_{B_s} + M_{D_s}} h_+ - \frac{\omega - 1}{M_{B_s} - M_{D_s}} h_- \right]. \end{aligned} \quad (2.11)$$

For $\bar{B}_s \rightarrow D_s^*$, the corresponding expressions for the vector-, axial- and tensor-current matrix elements have already been given in eq. (2.8).

In ref. [35], all the above form factors have been computed in the effective field theory, up to $\mathcal{O}(\alpha_s, \Lambda_{\text{QCD}}/m_{c,b})$ corrections, for the analogous $\bar{B} \rightarrow D^{(*)}$ semileptonic decays. We take advantage of this study and use the findings of ref. [35] to describe the $\bar{B}_s \rightarrow D_s^{(*)}$

form-factors. In the infinite heavy quark mass limit the form factors are given by the leading IW function $\xi(\omega)$ or they are zero. It is thus convenient to factor out the IW function and define $\hat{h}_i(\omega) = h_i(\omega)/\xi(\omega)$, which, up to $\mathcal{O}(\alpha_s, \Lambda_{\text{QCD}}/m_{c,b})$ corrections, read [35]

$$\begin{aligned}
 \hat{h}_{A_1} &= 1 + \hat{\alpha}_s C_{A_1} + \epsilon_c \left(\hat{L}_2 - \hat{L}_5 \frac{\omega - 1}{\omega + 1} \right) + \epsilon_b \left(\hat{L}_1 - \hat{L}_4 \frac{\omega - 1}{\omega + 1} \right), \\
 \hat{h}_{A_2} &= \hat{\alpha}_s C_{A_2} + \epsilon_c (\hat{L}_3 + \hat{L}_6), \\
 \hat{h}_{A_3} &= 1 + \hat{\alpha}_s (C_{A_1} + C_{A_3}) + \epsilon_c (\hat{L}_2 - \hat{L}_3 + \hat{L}_6 - \hat{L}_5) + \epsilon_b (\hat{L}_1 - \hat{L}_4), \\
 \hat{h}_V &= 1 + \hat{\alpha}_s C_{V_1} + \epsilon_c (\hat{L}_2 - \hat{L}_5) + \epsilon_b (\hat{L}_1 - \hat{L}_4), \\
 \hat{h}_{T_1} &= 1 + \hat{\alpha}_s \left[C_{T_1} + \frac{\omega - 1}{2} (C_{T_2} - C_{T_3}) \right] + \epsilon_c \hat{L}_2 + \epsilon_b \hat{L}_1 \\
 \hat{h}_{T_2} &= \hat{\alpha}_s \frac{\omega + 1}{2} (C_{T_2} + C_{T_3}) + \epsilon_c \hat{L}_5 - \epsilon_b \hat{L}_4 \\
 \hat{h}_{T_3} &= \hat{\alpha}_s C_{T_2} + \epsilon_c (\hat{L}_6 - \hat{L}_3) \\
 \hat{h}_+ &= 1 + \hat{\alpha}_s \left[C_{V_1} + \frac{\omega + 1}{2} (C_{V_2} + C_{V_3}) \right] + (\epsilon_c + \epsilon_b) \hat{L}_1,
 \end{aligned} \tag{2.12}$$

$$\hat{h}_- = \hat{\alpha}_s \frac{\omega + 1}{2} (C_{V_2} - C_{V_3}) + (\epsilon_c - \epsilon_b) \hat{L}_4. \tag{2.13}$$

The terms proportional to $\hat{\alpha}_s = \alpha_s/\pi$ are perturbative corrections computed by matching QCD to the HQET and, although dependent on ω , they are independent of the light degrees of freedom. The different $C_{A,V,T}$ functions can be found in appendix A of ref. [35]. In addition, $\epsilon_{c,b}$ are given by $\epsilon_{c,b} = \bar{\Lambda}/(2m_{c,b})$, with $\bar{\Lambda}$ a low energy constant (LEC) of order $\mathcal{O}(\Lambda_{\text{QCD}})$ for which we take the value quoted in ref. [35]. The six ω -dependent \hat{L}_j functions can be written in terms of just three sub-leading IW functions $\hat{\chi}_{2,3}$ and η (see eq. (8) in ref. [35]) for which the following near zero-recoil ($\omega = 1$) expansions are used³

$$\hat{\chi}_2(\omega) = \hat{\chi}_2(1) + \hat{\chi}'_2(1)(\omega - 1), \quad \hat{\chi}_3(\omega) = \hat{\chi}'_3(1)(\omega - 1), \quad \eta(\omega) = \eta(1) + \eta'(1)(\omega - 1) \tag{2.14}$$

Strictly speaking, $\bar{\Lambda}$ depends on the light-quark degrees of freedom. Thus, one expects some SU(3) breaking that will modify its value compared to that used in ref. [35] for $\bar{B} \rightarrow D^{(*)}$ decays. By keeping it the same, we reabsorb this change into the sub-leading IW functions which, together with the leading one, also suffer from SU(3) breaking effects.

For the leading IW function ξ we shall take the parametrization in ref. [43], where one has that

$$\xi(\omega) = 1 - 8\rho^2 \hat{z} + (64c - 16\rho^2) \hat{z}^2 + (256c - 24\rho^2 + 512d) \hat{z}^3 \tag{2.15}$$

and

$$\hat{z}(\omega) = \frac{\sqrt{\omega + 1} - \sqrt{2}}{\sqrt{\omega + 1} + \sqrt{2}}. \tag{2.16}$$

In addition, following ref. [43], we include the $\mathcal{O}[(\Lambda_{\text{QCD}}/m_c)^2]$ corrections introduced in ref. [44], which affect the form factors that are protected from $\mathcal{O}(\Lambda_{\text{QCD}}/m_c)$ corrections at zero recoil. In our case, not only \hat{h}_+ and \hat{h}_{A_1} but also h_{T_1} . We shall use

$$\hat{h}_+ \rightarrow \hat{h}_+ + \epsilon_c^2 l_1(1), \quad \hat{h}_{A_1} \rightarrow \hat{h}_{A_1} + \epsilon_c^2 l_2(1), \quad \hat{h}_{T_1} \rightarrow \hat{h}_{T_1} + \epsilon_c^2 l_3(1) \tag{2.17}$$

³In the case of $\hat{\chi}_3$ one has that $\hat{\chi}_3(1) = 0$ from Luke's theorem [42].

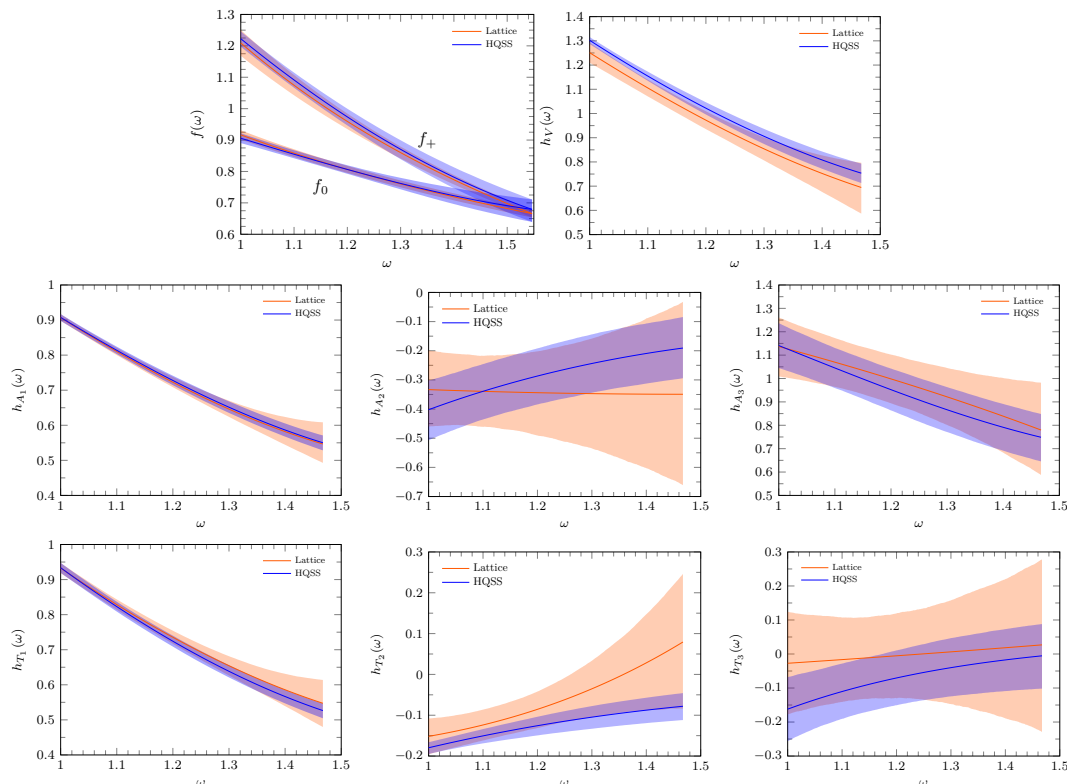


Figure 3. Comparison of the original LQCD form factors for $\bar{B}_s \rightarrow D_s$ [32] and $\bar{B}_s \rightarrow D_s^*$ [33] semileptonic decays and the HQET predictions after the fitting procedure described in the main text.

2.3 Fit of the SM-LQCD form factors to their HQSS/HQET expressions.

Treating the eleven HQET LECs $\rho^2, c, d, \hat{\chi}_2(1), \hat{\chi}'_2(1), \hat{\chi}'_3(1), \eta(1), \eta'(1), l_1(1), l_2(1)$ and $l_3(1)$ introduced above as free parameters, we can fit the LQCD form factors to their HQSS expressions. We fit the thirty-three independent coefficients a_i^F , with $F = +, 0, A_{1,2,3}, V, T_{1,2,3}$, that expand the LQCD form factors. The fit minimizes a χ^2 function, that in a simplified notation we can write as

$$\chi^2 = \sum_j \sum_k (a_j - f_j) C_{jk}^{-1} (a_k - f_k). \quad (2.18)$$

Here, the sum is over all the expansion coefficients, for which the a 's represent their central values, and the f 's stand for the expressions of the corresponding expansion coefficients in terms of the $\rho^2, c, d, \hat{\chi}_2(1), \hat{\chi}'_2(1), \hat{\chi}'_3(1), \eta(1), \eta'(1), l_1(1), l_2(1)$ and $l_3(1)$ best fit LECs. The f_j terms are obtained in the following way: for the D_s case we first multiply the HQSS form factors by the corresponding pole factors in eq. (2.6), and then we expand the result in powers of the z variable defined in eq. (2.7). For the D_s^* case, we directly expand the HQSS form factors in powers of $\omega - 1$. The covariance matrix C is block diagonal, built from the separate D_s and D_s^* covariance matrices compiled in tables 6 for $\bar{B}_s \rightarrow D_s$ and tables 9 to 13 for $\bar{B}_s \rightarrow D_s^*$ transitions respectively.

Since the LQCD results come from simulations on the same ensembles, with the same lattice actions and the same treatment of the chiral and continuum limits, we expect correlations

	$\bar{B}_s \rightarrow D_s^{(*)}$	$\bar{B}_s \rightarrow D_s^{(*)}$ (unc)	$\epsilon[\bar{B}_s \rightarrow D_s^{(*)}]$	$\bar{B} \rightarrow D^{(*)}$ [43]
ρ^2	1.29 ± 0.06	1.26 ± 0.07	0.07	1.32 ± 0.06
c	0.63 ± 0.24	0.53 ± 0.20	0.26	1.20 ± 0.12
d	0.15 ± 0.42	0.20 ± 0.37	0.42	-0.84 ± 0.17
$\hat{\chi}_2(1)$	-0.15 ± 0.13	-0.16 ± 0.11	0.13	-0.058 ± 0.020
$\hat{\chi}'_2(1)$	-0.15 ± 0.29	-0.50 ± 0.39	0.45	0.001 ± 0.020
$\hat{\chi}'_3(1)$	-0.03 ± 0.05	-0.04 ± 0.05	0.05	0.036 ± 0.020
$\eta(1)$	0.07 ± 0.12	0.13 ± 0.17	0.13	0.355 ± 0.040
$\eta'(1)$	-0.81 ± 0.28	0.28 ± 0.80	1.13	-0.03 ± 0.11
$l_1(1)$	0.04 ± 0.53	0.16 ± 0.53	0.54	0.14 ± 0.23
$l_2(1)$	-1.77 ± 0.30	-1.75 ± 0.30	0.30	-2.00 ± 0.30
$l_3(1)$	-2.86 ± 0.44	-2.91 ± 0.44	0.44	

Table 1. Second column: mean values and uncertainties of the $\rho^2, c, d, \hat{\chi}_2(1), \hat{\chi}'_2(1), \hat{\chi}'_3(1), \eta(1)$ and $\eta'(1)$ LECs obtained by fitting the $\bar{B}_s \rightarrow D_s^{(*)}$ LQCD form factors from refs. [32, 34] to their $\mathcal{O}(\alpha_s, \Lambda_{\text{QCD}}/m_{c,b})$ HQET expressions given in [35]. The first three parameters determine the leading IW function, while the last five enter in the $1/m_{c,b}$ sub-leading corrections. In addition, $l_1(1), l_2(1)$ and $l_3(1)$ account for $\mathcal{O}[(\Lambda_{\text{QCD}}/m_c)^2]$ contributions [44], which affect the \hat{h}_+, \hat{h}_{A_1} and \hat{h}_{T_1} form factors, respectively, which are protected from $\mathcal{O}(\Lambda_{\text{QCD}}/m_c)$ corrections at zero recoil. Third column: results from the totally uncorrelated fit, where we consider only the diagonal elements of the matrix C in the definition of the merit function of eq. (2.18). Fourth column: final total errors considered on the fitted LECs and used in the evaluation of the uncertainty bands for derived observables. They are computed by combining in quadrature the errors from the central fit (second column) with the magnitudes of the differences between the mean values of the central and uncorrelated fits. Fifth column: results for the analogous SU(3) fit carried out in ref. [43] to $\bar{B} \rightarrow D^{(*)}$ form-factor LQCD and experimental inputs. Note a typo (global sign) in the numerical value of $l_2(1)$ given in the original table 1 of ref. [43].

	ρ^2	c	d	$\hat{\chi}_2(1)$	$\hat{\chi}'_2(1)$	$\hat{\chi}'_3(1)$	$\eta(1)$	$\eta'(1)$	$l_1(1)$	$l_2(1)$	$l_3(1)$
ρ^2	1.000	0.595	-0.288	-0.241	0.231	0.286	0.074	-0.063	-0.015	-0.015	-0.017
c		1.000	-0.839	-0.221	0.440	-0.057	-0.022	0.051	0.102	0.021	0.015
d			1.000	0.082	0.042	0.330	0.037	-0.050	-0.287	-0.018	-0.015
$\hat{\chi}_2(1)$				1.000	-0.200	0.641	-0.222	-0.179	0.034	-0.009	-0.009
$\hat{\chi}'_2(1)$					1.000	0.284	-0.054	-0.053	-0.263	0.029	0.021
$\hat{\chi}'_3(1)$						1.000	0.007	0.001	-0.263	-0.033	-0.030
$\eta(1)$							1.000	0.211	0.125	-0.112	-0.085
$\eta'(1)$								1.000	-0.103	-0.026	-0.019
$l_1(1)$									1.000	-0.014	-0.010
$l_2(1)$										1.000	0.293
$l_3(1)$											1.000

Table 2. Correlation matrix of the $\rho^2, c, d, \hat{\chi}_2(1), \hat{\chi}'_2(1), \hat{\chi}'_3(1), \eta(1), \eta'(1), l_1(1), l_2(1)$ and $l_3(1)$ bestfit parameters after fitting the LQCD form factors from refs. [32, 33] to their $\mathcal{O}(\alpha_s, \Lambda_{\text{QCD}}/m_{c,b})$ HQET expressions.

between as well as within them. Lacking information on the former, we also tried fits with the D_s^* results taken as either fully correlated or fully anti-correlated with the D_s ones. That is, we augmented the correlation matrix corresponding to C with off-diagonal blocks for these two extreme cases with all entries taken to be either 1 or -1 . However, the new C matrices constructed in this way had negative eigenvalues. We also explored partially correlated scenarios (all matrix elements of the $D_s - D_s^*$ off-diagonal blocks set to r , with $|r| \leq 1$), but we found positive definite covariance matrices only for very small correlations $|r|$, of the percent order. Finally, we carried out a totally uncorrelated fit, where we considered only the diagonal elements of the matrix C in the definition of the merit function of eq. (2.18). That is to say, in this fit we also switched off the separate D_s^* and D_s correlations. The results for the central fitted parameters and errors are given in the second column of table 1, while the corresponding correlation matrix appears in table 2. The fit has $\chi^2/\text{dof} = 0.44$. We see the c and d coefficients are not determined with precision, which is probably a reflection of the large uncertainties in the lattice $\bar{B}_s \rightarrow D_s^*$ form factors at high ω values. Large uncertainties are also seen in the parameters of the sub-leading IW functions and $l_1(1)$. The next column shows the results from the totally uncorrelated fit (diagonal C matrix) which has $\chi^2/\text{dof} = 0.32$. The two fits give compatible results. We take the magnitude of the differences between the mean values of the central fit and those obtained in the uncorrelated (diagonal C matrix) fit as a further systematic error that we will combine in quadrature with the errors from the central fit to get our final error estimate for each of the parameters. Their values are presented in the next-to-last column of table 1. We retain the correlation matrix from the central fit (table 2). Using these ingredients we construct Gaussian distributions which are then used to compute 68% confidence level bands for derived observables.

In the final column of table 1, we include table 1 of [43], which contains the results for the analogous fit carried out in that work to $\bar{B} \rightarrow D^{(*)}$ LQCD and experimental form-factor inputs. For the two parameters that are better determined, ρ^2 and $l_2(1)$, we see small variations, compatible with the expected SU(3) light-flavor breaking corrections ($\sim 25 - 30\%$). For the others, all of them evaluated here with sizeable uncertainties, the differences between the central values in both fits are large. However, due to those sizable uncertainties, an interpretation as genuine unexpectedly-large SU(3)-breaking effects is very much limited.

A comparison of the original LQCD form factors from refs. [32, 34] and the HQET predictions after the fitting procedure just described is shown in figure 3. The LQCD error bands are notably much wider in most cases and we see a good agreement, within uncertainties, for all form-factors. The exception is h_V for ω values below 1.15 where the error bands hardly overlap.

In the next subsection, we show the different q^2 -distributions that fully determine the semileptonic $\bar{B}_s \rightarrow D_s^{(*)} \tau^- \bar{\nu}_\tau$ transitions for polarized final tau-leptons [45, 46].

2.4 Visible kinematics of the sequential $H_b \rightarrow H_c \tau^- (\pi^- \nu_\tau, \rho^- \nu_\tau, \ell^- \bar{\nu}_\ell \nu_\tau) \bar{\nu}_\tau$ decays

If the spins of the $H_{b,c}$ hadrons are not measured, the ideal experiment to obtain the maximum information would be one in which both the momentum and spin (or helicity) state of the τ lepton could be established. This is however not possible since the τ is very short-lived.

Thus, information about the $H_b \rightarrow H_c \tau^- \bar{\nu}_\tau$ parent decay has to be accessed via the visible kinematics of the τ decay products.

We have considered the three τ decay channels $\tau^- \rightarrow \pi^- \nu_\tau$, $\rho^- \nu_\tau$ and $\ell^- \bar{\nu}_\ell \nu_\tau$, with $\ell = \mu, e$, that account for up to 70% of the total τ decay width. Of the τ -decay products, only the charged particle $d = \pi^-, \rho^-$ or ℓ^- will be observed and, in the zero τ -width limit, one can write the differential decay width [46–49]

$$\frac{d^3\Gamma_d}{d\omega d\xi_d d \cos\theta_d} = \mathcal{B}_d \frac{d\Gamma_{\text{SL}}}{d\omega} \left\{ F_0^d(\omega, \xi_d) + F_1^d(\omega, \xi_d) \cos\theta_d + F_2^d(\omega, \xi_d) P_2(\cos\theta_d) \right\}. \quad (2.19)$$

As already mentioned, ω is the product of the four-velocities of the H_b and H_c hadrons, which is related to the four-momentum transfer squared q^2 through the relation $q^2 = M^2 + M'^2 - 2MM'\omega$, with $M(M')$ the mass of the $H_b(H_c)$ hadron. In addition, ξ_d is the ratio of the d charged particle and τ energies measured in the $\tau^- \bar{\nu}_\tau$ center of mass frame (CM), while θ_d is the angle made by the three-momenta of the d charged particle and the H_c final hadron, also measured in the CM frame (for the kinematics, see for instance figure 1 of ref. [50]). \mathcal{B}_d is the branching ratio for the corresponding τ decay mode and P_2 stands for the Legendre polynomial of order two. In addition, $d\Gamma_{\text{SL}}/d\omega$ accounts for the unpolarized $H_b \rightarrow H_c \tau^- \bar{\nu}_\tau$ decay width that can be written as [50]

$$\frac{d\Gamma_{\text{SL}}}{d\omega} = \frac{G_F^2 |V_{cb}|^2 M'^3 M^2}{24\pi^3} \sqrt{\omega^2 - 1} \left(1 - \frac{m_\tau^2}{q^2}\right)^2 n_0(\omega), \quad (2.20)$$

with G_F the Fermi decay constant and V_{cb} the corresponding Cabibbo-Kobayashi-Maskawa matrix element. The $n_0(\omega)$ function contains all the dynamical information, including possible NP effects. Finally, the $F_{0,1,2}^d(\omega, \xi_d)$ functions read [46]

$$\begin{aligned} F_0^d(\omega, \xi_d) &= C_n^d(\omega, \xi_d) + C_{P_L}^d(\omega, \xi_d) \langle P_L^{\text{CM}} \rangle(\omega), \\ F_1^d(\omega, \xi_d) &= C_{A_{FB}}^d(\omega, \xi_d) A_{FB}(\omega) + C_{Z_L}^d(\omega, \xi_d) Z_L(\omega) + C_{P_T}^d(\omega, \xi_d) \langle P_T^{\text{CM}} \rangle(\omega), \\ F_2^d(\omega, \xi_d) &= C_{A_Q}^d(\omega, \xi_d) A_Q(\omega) + C_{Z_Q}^d(\omega, \xi_d) Z_Q(\omega) + C_{Z_\perp}^d(\omega, \xi_d) Z_\perp(\omega). \end{aligned} \quad (2.21)$$

with $C_a^d(\omega, \xi_d)$ kinematical coefficients that are decay-mode dependent and whose expressions can be found in appendix G of ref. [46]. The rest of the observables in eq. (2.21) represent spin ($\langle P_{L,T}^{\text{CM}} \rangle(\omega)$), angular ($A_{FB,Q}(\omega)$) and spin-angular ($Z_{L,Q,\perp}(\omega)$) asymmetries of the $H_b \rightarrow H_c \tau^- \bar{\nu}_\tau$ parent decay [46]. In the absence of CP-odd contributions, these asymmetries, together with $d\Gamma_{\text{SL}}/d\omega$, encode the maximal information obtainable if one could directly analyze the polarized $H_b \rightarrow H_c \tau^- \bar{\nu}_\tau$ transitions (see ref. [45] and especially eq. (3.46) of ref. [46] and the related discussion). All the above observables (n_0 , $\langle P_{L,T}^{\text{CM}} \rangle$, $A_{FB,Q}$ and $Z_{L,Q,\perp}$) are determined by the matrix elements of the $b \rightarrow c$ current between the initial (H_b) and final (H_c) hadrons. After summing over hadron polarizations the hadron tensors can be expressed in terms of Lorentz scalar structure functions, which depend on q^2 or equivalently on ω , the hadron masses and some Wilson coefficients if physics beyond the SM is considered. Lorentz, parity and time-reversal transformations of the hadron currents and states limit their number, as discussed in detail in ref. [51]. The discussion of subsection 2.2 of ref. [46] shows how to get the unpolarized $d\Gamma_{\text{SL}}/d\omega$ distribution and the tau spin, angular and spin-angular asymmetries in terms of general structure functions which can be obtained from the matrix

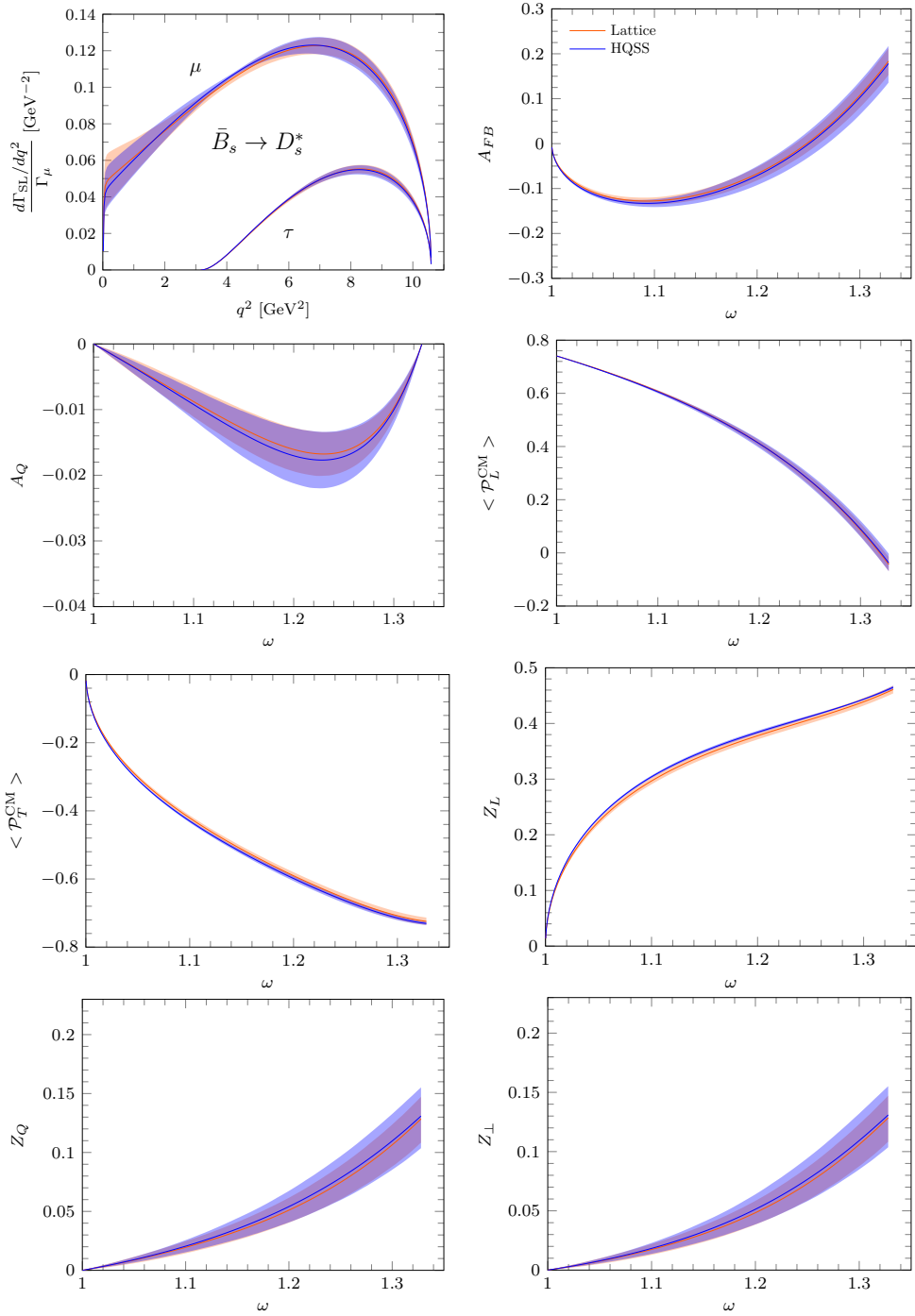


Figure 4. $d\Gamma_{\text{SL}}/dq^2$ differential decay width, divided by $\Gamma_\mu = \Gamma(\bar{B}_s \rightarrow D_s^* \mu^- \bar{\nu}_\mu)$, and the different tau-asymmetries introduced in eq. (2.21) for the semileptonic $\bar{B}_s \rightarrow D_s^* \tau \bar{\nu}_\tau$ decay. We compare the results evaluated with the SM-LQCD form factors from refs. [32, 33] and with the SM-HQET form factors obtained after the fitting procedure described in subsection 2.3.

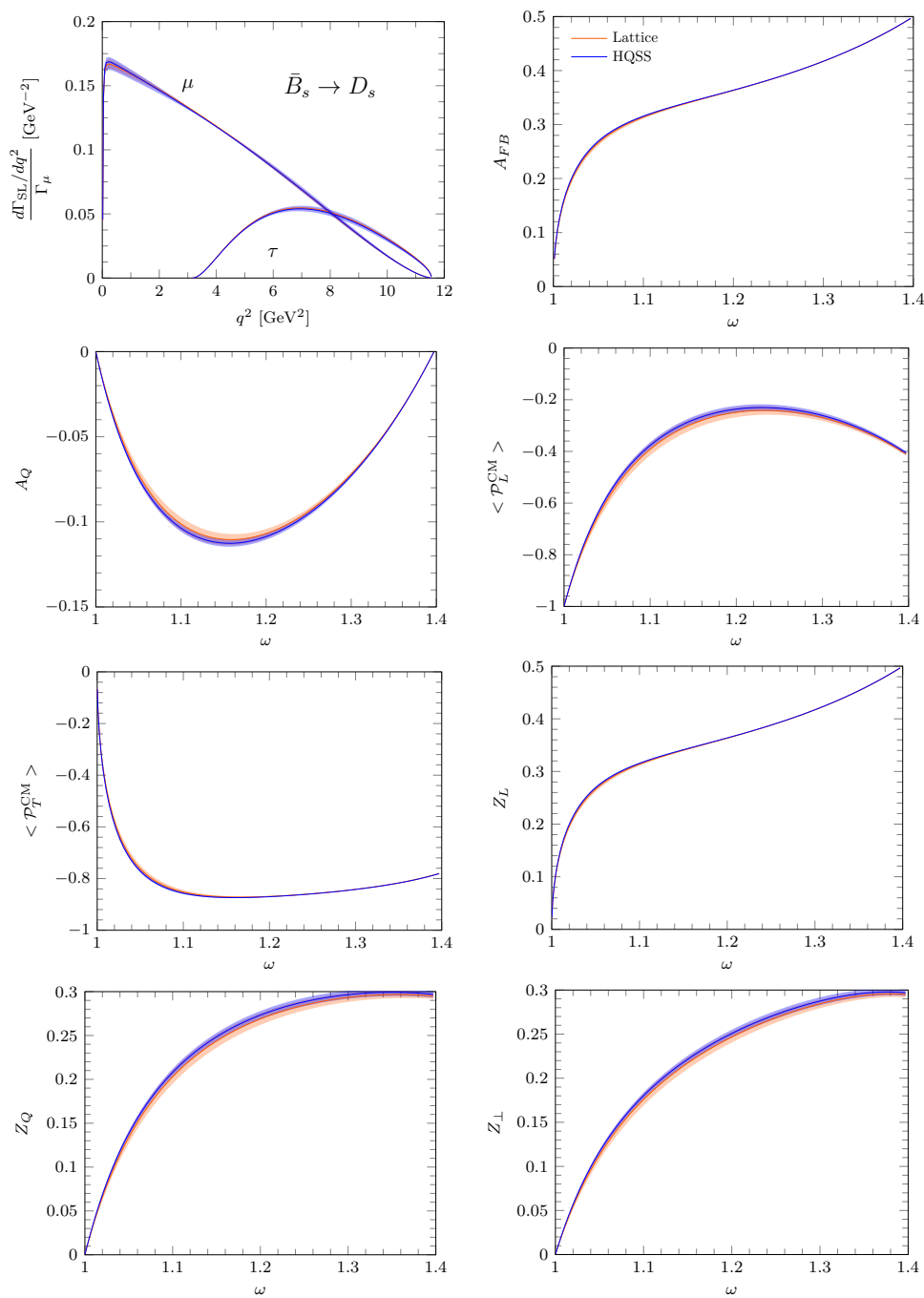


Figure 5. Same as figure 4 for the $\bar{B}_s \rightarrow D_s$ semileptonic decay.

elements of the relevant hadron operators. The matrix elements are in turn parametrized in terms of form-factors. The findings of refs. [46, 51] are quite general and can be applied not only to the SM but also to any extension of the SM based on the low-energy effective Hamiltonian comprising the full set of dimension-6 semileptonic $b \rightarrow c\tau\bar{\nu}_\tau$ operators with left- and right-handed neutrino fields.

For pseudoscalar meson decay into pseudoscalar or vector mesons, the relations between structure functions and form factors can be found in appendix B of ref. [52].

In figures 4 and 5 we show, for the $\bar{B}_s \rightarrow D_s^*$ and $\bar{B}_s \rightarrow D_s$ semileptonic decays respectively, the results for the SM $d\Gamma/dq^2$ differential decay width and the different asymmetries, introduced above, that can be obtained from the measurement of the visible kinematics of the charged τ -decay product. Only the differential $d\Gamma/dq^2$ distribution was shown in the original LQCD work of ref. [32] ([34]) for $\bar{B}_s \rightarrow D_s$ ($\bar{B}_s \rightarrow D_s^*$). The tau forward-backward angular A_{FB} and spin $\langle P_L^{CM} \rangle$ asymmetries were also presented for $\bar{B}_s \rightarrow D_s^*$ in ref. [33] but with lattice form factors that have now been superseded by the new ones evaluated in ref. [34]. The rest of the observables are shown here for the very first time for the SM in figures 4 and 5 and for some extensions of the SM in the next section. As for figures 4 and 5, they have been evaluated both with the SM-LQCD form factors from refs. [32, 33] and with the SM-HQET form factors obtained in subsection 2.3. The two results agree within uncertainties in all cases.

All this gives us confidence in the quality of the fitted HQET IW functions so that we can go a step further and use the relations in ref. [35] to obtain in addition the HQSS scalar and pseudoscalar form factors of the two $\bar{B}_s \rightarrow D_s^{(*)}$ semileptonic transitions and the tensor one for the $\bar{B}_s \rightarrow D_s$ decay. Such a scheme relies on eqs. (14) and (15) of ref. [35] and it also properly includes short-distance and $1/m_{c,b}$ [$\mathcal{O}(\alpha_s, \Lambda_{\text{QCD}}/m_{c,b})$] corrections for the NP form-factors. Using the full set of HQSS form factors we can address, in the next section, the possibility of NP effects in these two decays.

3 New physics effects in $\bar{B}_s \rightarrow D_s^{(*)}\tau^-\nu_\tau$ semileptonic decays

Following ref. [53], to account for NP effects in a model independent way, we shall take a phenomenological effective field theory approach in which we consider all dimension-six $b \rightarrow c\tau\bar{\nu}_\tau$ semileptonic operators (see section 3.1 below). These effective low energy operators are assumed to be generated by BSM physics that enters at a much higher energy scale. Their strengths are governed by Wilson coefficients (WCs) that can be fitted to experimental data. This data typically includes the $\mathcal{R}_{D^{(*)}} = \Gamma(B \rightarrow D^{(*)}\tau^-\bar{\nu}_\tau)/\Gamma(B \rightarrow D^{(*)}\mu^-\bar{\nu}_\mu)$ ratios, the tau longitudinal polarization asymmetry and the longitudinal D^* polarization (also measured by Belle [5, 54]), the τ forward-backward asymmetry and the upper bound for the $\bar{B}_c \rightarrow \tau\bar{\nu}_\tau$ decay rate [55]. There have been a large number of calculations along these lines, for the $\bar{B} \rightarrow D^{(*)}$ [35, 43, 45, 52, 53, 56–71], $\bar{B}_c \rightarrow J/\psi, \eta_c$ [22, 24, 52, 72, 73], $\Lambda_b \rightarrow \Lambda_c$ [43, 45, 51, 63, 74–87] and⁴ $\Lambda_b \rightarrow \Lambda_c(2595), \Lambda_c(2625)$ [79, 88, 89, 92–95] semileptonic decays.

⁴The isoscalar $\Lambda_c(2595)$ and $\Lambda_c(2625)$, with $J^P = 1/2^-$ and $3/2^-$ respectively, are promising candidates for the lightest heavy-quark-spin doublet of negative-parity charmed-baryon resonances [88–90], although some reservations are given in [91]. Experimental distributions for the semileptonic decay of the ground-state bottom baryon Λ_b into both excited states would definitely help shed light on this issue [90].

Here, profiting from the lattice determination of the $\bar{B}_s \rightarrow D_s$ SM form factors [32] and the $\bar{B}_s \rightarrow D_s^*$ SM and tensor form factors [34], together with the HQET study of $\bar{B} \rightarrow D^{(*)}$ form factors in ref. [35], we have obtained all the $\bar{B}_s \rightarrow D_s^{(*)}$ form factors needed for a similar study of the $\bar{B}_s \rightarrow D_s^{(*)} \tau \bar{\nu}_\tau$ semileptonic decays. If NP is responsible for LFUV, one would expect to see its effects in these reactions at a level similar to that found in the analogous $\bar{B} \rightarrow D^{(*)}$ decays. In addition to the $\mathcal{R}_{D_s^{(*)}} = \Gamma(\bar{B} \rightarrow D_s^{(*)} \tau \bar{\nu}_\tau) / \Gamma(\bar{B}_s \rightarrow D_s^{(*)} \ell \bar{\nu}_\ell)$ ratios, we will investigate the role that the different asymmetries presented in subsection 2.4 could play in establishing the presence of LFUV and, if experimentally confirmed, to distinguish between different extensions of the SM.

3.1 $H_b \rightarrow H_c \ell^- \bar{\nu}_\ell$ Effective Hamiltonian

The effective low-energy Hamiltonian that we use follows ref. [68] and it includes all possible dimension-six semileptonic $b \rightarrow c$ operators with both left-handed (L) and right-handed (R) neutrino fields,

$$H_{\text{eff}} = \frac{4G_F V_{cb}}{\sqrt{2}} \left[(1 + C_{LL}^V) \mathcal{O}_{LL}^V + C_{RL}^V \mathcal{O}_{RL}^V + C_{LL}^S \mathcal{O}_{LL}^S + C_{RL}^S \mathcal{O}_{RL}^S + C_{LL}^T \mathcal{O}_{LL}^T \right. \\ \left. + C_{LR}^V \mathcal{O}_{LR}^V + C_{RR}^V \mathcal{O}_{RR}^V + C_{LR}^S \mathcal{O}_{LR}^S + C_{RR}^S \mathcal{O}_{RR}^S + C_{RR}^T \mathcal{O}_{RR}^T \right] + h.c.. \quad (3.1)$$

Here, the C_{AB}^X ($X = S, V, T$ and $A, B = L, R$) are, complex in general, Wilson coefficients that parameterize the deviations from the SM. They can be lepton and flavor dependent although they are generally assumed to be nonzero only for the third quark and lepton generation. The dimension six operators read

$$\mathcal{O}_{(L,R)L}^V = (\bar{c} \gamma^\mu b_{L,R}) (\bar{\ell} \gamma_\mu \nu_{\ell L}), \quad \mathcal{O}_{(L,R)L}^S = (\bar{c} b_{L,R}) (\bar{\ell} \nu_{\ell L}), \quad \mathcal{O}_{LL}^T = (\bar{c} \sigma^{\mu\nu} b_L) (\bar{\ell} \sigma_{\mu\nu} \nu_{\ell L}), \quad (3.2)$$

$$\mathcal{O}_{(L,R)R}^V = (\bar{c} \gamma^\mu b_{L,R}) (\bar{\ell} \gamma_\mu \nu_{\ell R}), \quad \mathcal{O}_{(L,R)R}^S = (\bar{c} b_{L,R}) (\bar{\ell} \nu_{\ell R}), \quad \mathcal{O}_{RR}^T = (\bar{c} \sigma^{\mu\nu} b_R) (\bar{\ell} \sigma_{\mu\nu} \nu_{\ell R}), \quad (3.3)$$

with $\psi_{R,L} = (1 \pm \gamma_5) \psi / 2$. The effective Hamiltonian can be rewritten as [46]

$$H_{\text{eff}} = \frac{4G_F V_{cb}}{\sqrt{2}} \sum_{\chi=L,R} \left[\bar{c} (C_\chi^V \gamma^\mu + h_\chi C_\chi^A \gamma^\mu \gamma_5) b \bar{\ell} \gamma_\mu \nu_{\ell \chi} + \bar{c} (C_\chi^S + h_\chi C_\chi^P \gamma_5) b \bar{\ell} \gamma_\mu \nu_{\ell \chi} \right. \\ \left. + C_\chi^T \bar{c} \sigma^{\mu\nu} (1 + h_\chi \gamma_5) b \bar{\ell} \sigma_{\mu\nu} \nu_{\ell \chi} \right] \quad (3.4)$$

with $h_L = -1, h_R = +1$ and

$$C_L^V = (1 + C_{LL}^V + C_{RL}^V), \quad C_L^A = (1 + C_{LL}^V - C_{RL}^V), \\ C_L^S = (C_{LL}^S + C_{RL}^S), \quad C_L^P = (C_{LL}^S - C_{RL}^S), \quad C_L^T = C_{LL}^T, \\ C_R^V = (C_{LR}^V + C_{RR}^V), \quad C_R^A = -(C_{LR}^V - C_{RR}^V), \\ C_R^S = (C_{LR}^S + C_{RR}^S), \quad C_R^P = -(C_{LR}^S - C_{RR}^S), \quad C_R^T = C_{RR}^T, \quad (3.5)$$

We shall compare results obtained in the SM and in three different NP extensions. The latter correspond to the L Fit 7 of ref. [43], where only left-handed neutrino operators are considered, the R S7a scenario of ref. [68] with only right-handed neutrino operators, and

the left-handed neutrino $L R_2$ leptoquark model of ref. [66], for which the two nonzero WCs (C_{LL}^S and C_{LL}^T) are complex.⁵ In this latter case the effective Hamiltonian violates CP.

None of the observables $d\Gamma_{\text{SL}}/d\omega$, $\langle P_{L,T}^{\text{CM}} \rangle$, $A_{FB,Q}$ and $Z_{L,Q,\perp}$ entering eqs. (2.19) and (2.21) are sensitive to CP-symmetry breaking terms [45, 46]. Hence, we will also show results for the $L R_2$ leptoquark model of ref. [66] for other distributions, related to the tau polarization component (P_{TT}) along an axis perpendicular to the hadron-tau plane [45], which could be accessed if one could further measure the azimuthal angle (ϕ_d) of the charged d particle (see figure 1 of ref. [50]). Note that in the differential distribution given in eq. (2.19) this angle has been integrated out since measuring ϕ_d would require a full reconstruction of the tau three-momentum. The latter can be circumvented through the analysis of distributions that also involve the decay products of the H_c hadron. Thus, some CP-odd observables have been presented for $\bar{B} \rightarrow D^*$ and $\Lambda_b \rightarrow \Lambda_c$ decays in refs. [58, 59, 61, 71] and refs. [83, 85] respectively.

As already mentioned, we refer the reader to ref. [46], and references therein, for a full account of our formalism.

3.2 Partially integrated sequential $H_b \rightarrow H_c \tau^- (\pi^- \nu_\tau, \rho^- \nu_\tau, \ell^- \bar{\nu}_\ell \nu_\tau) \bar{\nu}_\tau$ decay distributions

The feasibility of NP studies can be severely limited, however, by the statistical precision in the measurement of the triple differential decay width of eq. (2.19). One can increase statistics, at the expense of losing information in some of the observables, by integrating over one or more of the ω , ξ_d and θ_d variables, although in this case not all observables entering in eq. (2.21) can be extracted. In this way one can obtain the distributions [50]

$$\frac{d^2\Gamma_d}{d\omega d\xi_d} = 2\mathcal{B}_d \frac{d\Gamma_{\text{SL}}}{d\omega} \left\{ C_n^d(\omega, \xi_d) + C_{P_L}^d(\omega, \xi_d) \langle P_L^{\text{CM}} \rangle(\omega) \right\}, \quad (3.6)$$

from which only $d\Gamma_{\text{SL}}/d\omega$ and the CM τ longitudinal polarization can be extracted, or

$$\frac{d^2\Gamma_d}{d\omega d\cos\theta_d} = \mathcal{B}_d \frac{d\Gamma_{\text{SL}}}{d\omega} \left[\frac{1}{2} + \tilde{F}_1^d(\omega) \cos\theta_d + \tilde{F}_2^d(\omega) P_2(\cos\theta_d) \right], \quad (3.7)$$

with

$$\tilde{F}_1^d(\omega) = C_{A_{FB}}^d(\omega) A_{FB}(\omega) + C_{Z_L}^d(\omega) Z_L(\omega) + C_{P_T}^d(\omega) \langle P_T^{\text{CM}} \rangle(\omega), \quad (3.8)$$

$$\tilde{F}_2^d(\omega) = C_{A_Q}^d(\omega) A_Q(\omega) + C_{Z_Q}^d(\omega) Z_Q(\omega) + C_{Z_\perp}^d(\omega) Z_\perp(\omega), \quad (3.9)$$

which retains information on $d\Gamma_{\text{SL}}/dq^2$ and six out of the seven original asymmetries. The latter cannot, however, be extracted from the knowledge of \tilde{F}_1^d and \tilde{F}_2^d alone.

One can further integrate over ω to obtain [50]

$$\frac{d\Gamma_d}{d\cos\theta_d} = \mathcal{B}_d \Gamma_{\text{SL}} \left[\frac{1}{2} + \hat{F}_1^d \cos\theta_d + \hat{F}_2^d P_2(\cos\theta_d) \right], \quad \hat{F}_{1,2}^d = \frac{1}{\Gamma_{\text{SL}}} \int_1^{\omega_{\text{max}}} \frac{d\Gamma_{\text{SL}}}{d\omega} \tilde{F}_{1,2}^d(\omega) d\omega. \quad (3.10)$$

⁵The numerical values that we use for these two WCs can be found at the beginning of subsection 4.2.1 of ref. [45].

and

$$\frac{d\Gamma_d}{dE_d} = 2\mathcal{B}_d \int_{\omega_{\text{inf}}(E_d)}^{\omega_{\text{sup}}(E_d)} d\omega \frac{1}{\gamma m_\tau} \frac{d\Gamma_{\text{SL}}}{d\omega} \left\{ C_n^d(\omega, \xi_d) + C_{P_L}^d(\omega, \xi_d) \langle P_L^{\text{CM}} \rangle(\omega) \right\}, \quad (3.11)$$

where $\gamma = (q^2 + m_\tau^2)/(2m_\tau\sqrt{q^2})$ and, in the latter case, the appropriate ω limits can be found in ref. [50].

Although the information on the individual asymmetries is now completely lost, the above two distributions could still be useful observables in the search for NP beyond the SM.

3.3 NP results and discussion

3.3.1 LFUV ratios, unpolarized differential decay widths and tau angular, spin and spin-angular asymmetries

We start by showing, in table 3, the values for the semileptonic decay widths $\Gamma_\tau = \Gamma(\bar{B}_s \rightarrow D_s^{(*)} \tau \bar{\nu}_\tau)$ and $\Gamma_\ell = \Gamma(\bar{B}_s \rightarrow D_s^{(*)} \ell \bar{\nu}_\ell)$, with $\ell = e, \mu$, and the corresponding $\mathcal{R}_{D_s^{(*)}}$ ratios, evaluated within the SM and the three NP extensions, L Fit 7 of ref. [43], R S7a scenario of ref. [68] and the L R_2 leptoquark model of ref. [66], considered in this study. Our results for the SM ratios are compatible with those obtained using a dispersive matrix approach in [96]. Both use HPQCD lattice data, but our values make use of the updated values from [34]; we find that the agreement is closer if we base our analysis on the same HPQCD inputs [32, 33] as used in [96].⁶ For the first two NP models, we clearly see the ratios deviate from the SM prediction.⁷ Their central values are higher than SM ones, with the highest one corresponding always to L Fit 7, which leads to ratios around 5σ above the SM predictions. The results are similar to those obtained in ref. [50] for the analogous $\bar{B} \rightarrow D^{(*)}$ decays (see table 3 of that reference). In the L R_2 case, $\mathcal{R}_{D_s^*}$ is larger than the SM value while \mathcal{R}_{D_s} is lower and compatible within errors.

In figures 6 and 7 we show now the values for the $n_0(\omega)$ function introduced in eq. (2.20), which contains all the dynamical information of the $d\Gamma_{\text{SL}}/d\omega$ differential decay width, and the set of tau spin, angular and spin-angular asymmetries introduced in eq. (2.21). Most of the observables allow for a clear distinction between SM and L Fit 7 results, the exception being the CM longitudinal spin asymmetry $\langle P_L^{\text{CM}} \rangle$ for the $\bar{B}_s \rightarrow D_s^*$ decay. In fact, these observables also differentiate between L Fit 7 and the other two NP scenarios. With few exceptions, notably the Z_Q and Z_\perp asymmetries for the $\bar{B}_s \rightarrow D_s$ decays, the R S7a and L R_2 NP scenarios tend to agree within errors and they are closer to the SM, especially in the case of the L R_2 model.

As already mentioned, none of the observables shown so far is sensitive to CP breaking terms. To measure those one needs to analyze the CP violating triple product asymmetries that involve the decay of the H_c hadron [58, 59, 61, 71, 83, 85], or otherwise to be able to fully establish the tau three-momentum. In the latter case, one has access to the $\langle P_{TT}^{\text{CM}} \rangle(\omega)$

⁶The updated HPQCD results in [34] have been used in the dispersive matrix method for $\bar{B} \rightarrow D^*$ semileptonic decays in [97], but not yet used for $\bar{B}_s \rightarrow D_s^*$.

⁷The LQCD results in refs. [32] and [34] are $\mathcal{R}_{D_s^*}^{\text{SM}} = 0.2993(46)$ and $\mathcal{R}_{D_s}^{\text{SM}} = 0.265(9)$, which are in excellent agreement with the prediction quoted in table 3 obtained with the HQET parameterization of the $\bar{B}_s \rightarrow D_s^{(*)}$ form-factors.

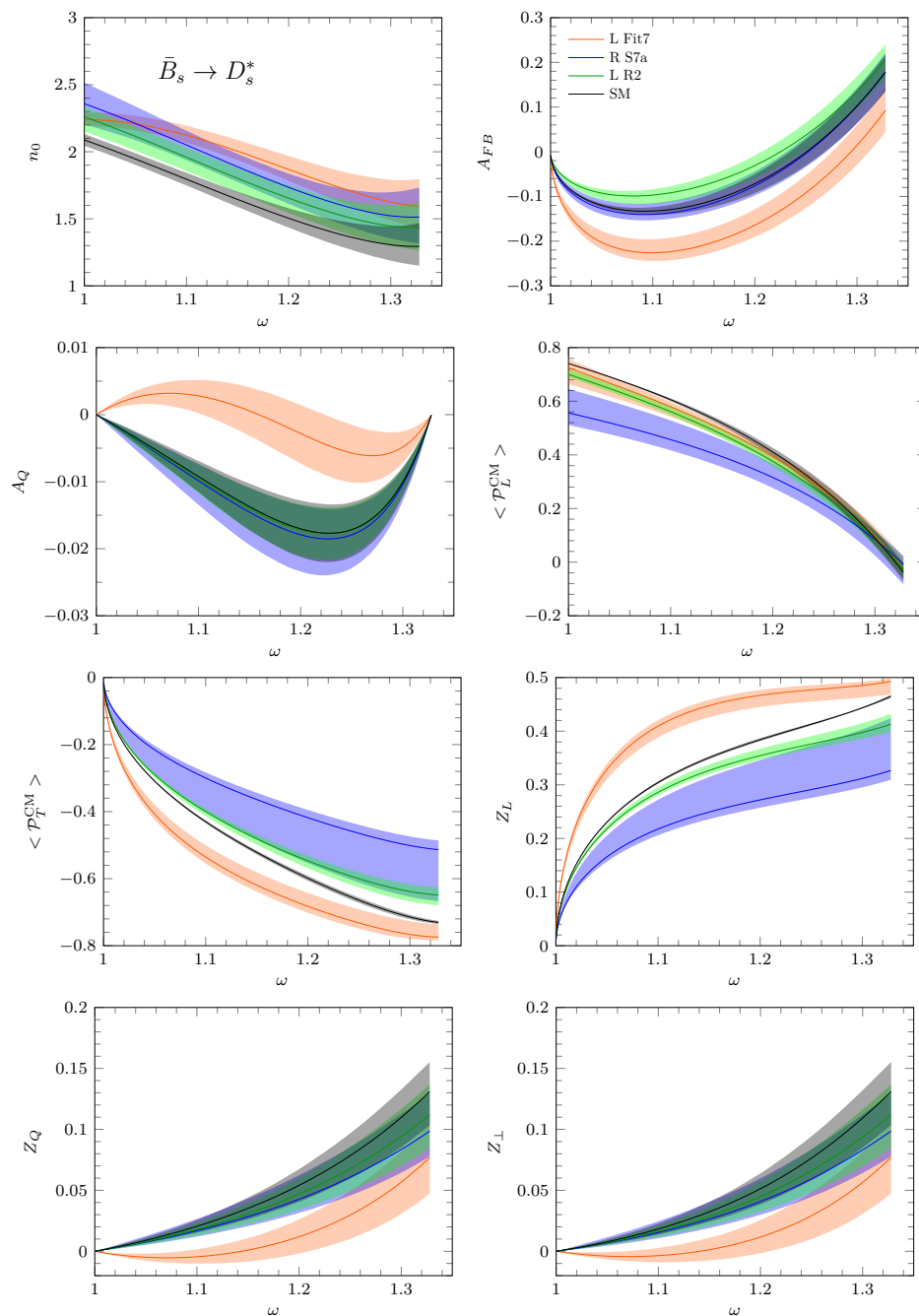


Figure 6. Distribution n_0 from eq. (2.20) and the tau asymmetries introduced in eq. (2.21) for the $\bar{B}_s \rightarrow D_s^* \tau \bar{\nu}_\tau$ decay. We compare the results for these observables obtained in the SM and the NP models L Fit 7, R S7a and L R_2 of refs. [43], [68] and [66], respectively. We use the HQET form-factors derived from the LQCD form factors obtained in refs. [32, 34].

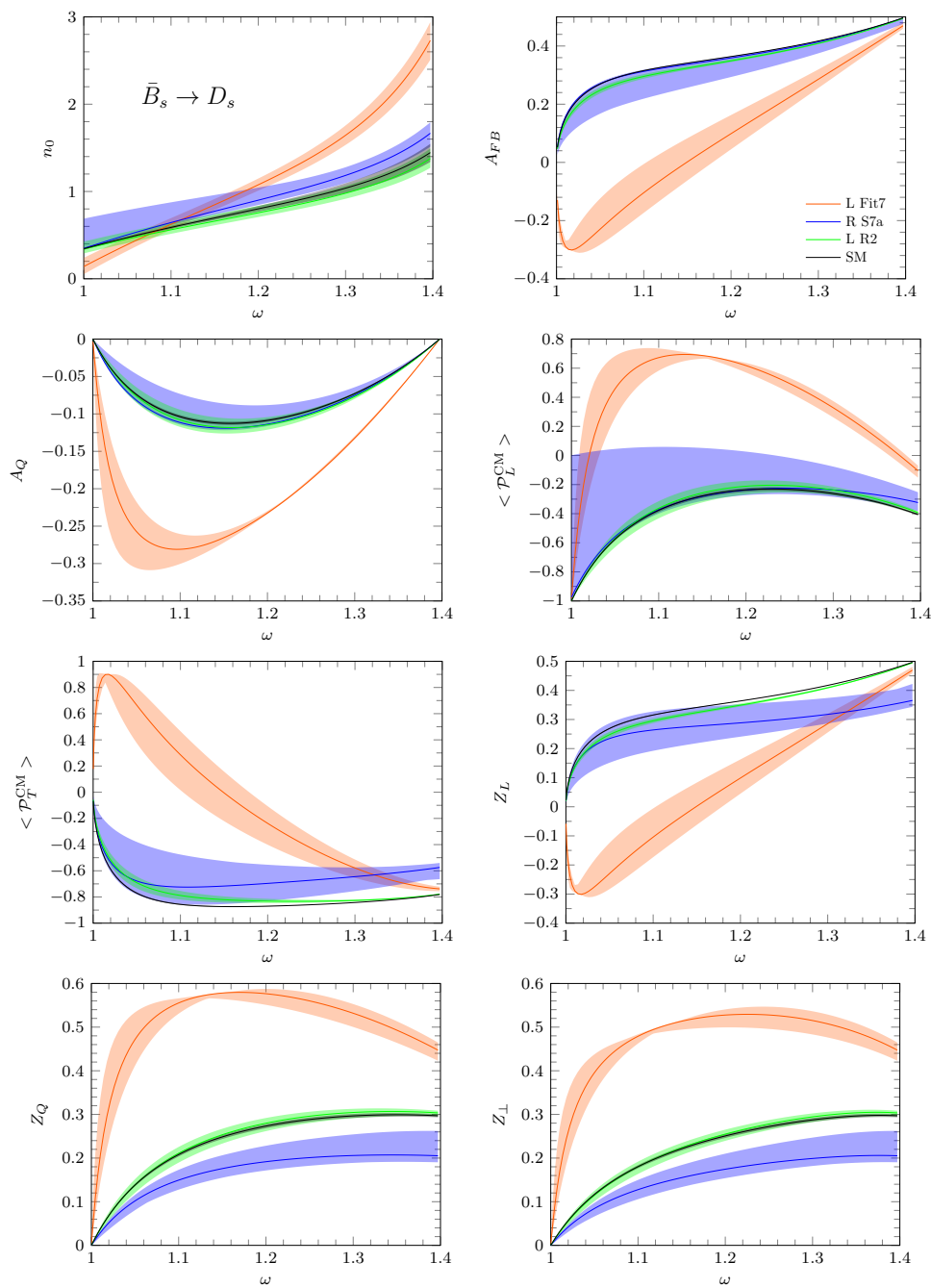


Figure 7. Same as figure 6 but for the $\bar{B}_s \rightarrow D_s \tau \bar{\nu}_\tau$ transition.

		SM	L Fit 7 [43]	R S7a [68]	L R_2 [66]
Distribution	$\bar{B}_s \rightarrow D_s$	$0.93^{+0.07}_{-0.08}$			
	$\Gamma_{e(\mu)}$				
	Γ_τ	0.27 ± 0.01	0.36 ± 0.02	$0.306^{+0.062}_{-0.019}$	$0.259^{+0.022}_{-0.015}$
	\mathcal{R}_{D_s}	$0.295^{+0.015}_{-0.011}$	$0.387^{+0.024}_{-0.019}$	$0.329^{+0.067}_{-0.018}$	$0.279^{+0.026}_{-0.015}$
$\bar{B}_s \rightarrow D_s^*$	$\Gamma_{e(\mu)}$	$1.91^{+0.13}_{-0.10}$			
	Γ_τ	$0.507^{+0.018}_{-0.015}$	$0.605^{+0.025}_{-0.023}$	$0.581^{+0.031}_{-0.033}$	$0.554^{+0.020}_{-0.018}$
	$\mathcal{R}_{D_s^*}$	$0.265^{+0.009}_{-0.010}$	$0.316^{+0.014}_{-0.015}$	$0.304^{+0.016}_{-0.019}$	0.290 ± 0.019

Table 3. Semileptonic decay widths $\Gamma_\tau = \Gamma(\bar{B}_s \rightarrow D_s^{(*)} \tau \bar{\nu}_\tau)$ and $\Gamma_{e(\mu)} = \Gamma[\bar{B}_s \rightarrow D_s^{(*)} e(\mu) \bar{\nu}_{e(\mu)}]$ (in units of $10 \times |V_{cb}|^2 \text{ps}^{-1}$) and ratios $\mathcal{R}_{D_s^{(*)}} = \Gamma(\bar{B}_s \rightarrow D_s^{(*)} \tau \bar{\nu}_\tau) / \Gamma[\bar{B}_s \rightarrow D_s^{(*)} e(\mu) \bar{\nu}_{e(\mu)}]$ obtained using the SM-HQSS form factors, the NP model L Fit 7 (R S7a) of ref. [43] ([68]), which only includes left-(right-)handed neutrino NP operators and the L R_2 leptoquark model of ref. [66]. Errors induced by the uncertainties in the form-factors and Wilson coefficients are added in quadrature.

observable, which gives the component of the CM tau-polarization vector along an axis perpendicular to the hadron-tau plane (see eqs. (3.14), (3.24) and (3.25) of ref. [45]). Among the different NP extensions considered in this work, only the L R_2 leptoquark model of ref. [66], with complex Wilson coefficients, can generate a nonzero value for the $\langle P_{TT}^{\text{CM}} \rangle(\omega)$ distribution. In this NP model, the two nonzero WCs C_{LL}^S and C_{LL}^T are given, at the bottom-mass scale appropriate for the present calculation, in terms of just the value of C_{LL}^T at the 1 TeV scale, where $C_{LL}^S(1 \text{ TeV}) = 4C_{LL}^T(1 \text{ TeV})$, and the corresponding evolution matrix (see ref. [66]). The best fit of the WCs to the \bar{B} -meson LFUV signatures does not fix the sign of the imaginary part of $C_{LL}^T(1 \text{ TeV})$. Contrary to the other observables considered so far, $\langle P_{TT}^{\text{CM}} \rangle(\omega)$ is linear in this imaginary part and thus its measurement would break this degeneracy. The results for $\langle P_{TT}^{\text{CM}} \rangle(\omega)$, using both possible signs for $\text{Im}[C_{LL}^T(1 \text{ TeV})]$, are shown in the upper panels of figure 8 for the $\bar{B}_s \rightarrow D_s^*$ (left) and $\bar{B}_s \rightarrow D_s$ (right) decays respectively. We see that the absolute value of this distribution is around one order of magnitude larger for the pseudoscalar than for the vector decay modes. An observation of a nonzero $\langle P_{TT}^{\text{CM}} \rangle(\omega)$ value will be a clear indication of the existence of NP beyond the SM and CP violation.

In the bottom panel of figure 8 we show the degree of polarization of the tau

$$\langle P^2 \rangle(\omega) = -\langle P_L^2 + P_T^2 + P_{TT}^2 \rangle(\omega) \tag{3.12}$$

which is a Lorentz invariant quantity. As shown in ref. [45], this is exactly -1 for $0^- \rightarrow 0^-$ transitions, reflecting the fact that for such decays the outgoing taus are fully polarized. Thus we only present the results for the $\bar{B}_s \rightarrow D_s^*$ decay. As seen from the figure this observable, which is sensitive to CP-odd terms in the effective Hamiltonian, discriminates very efficiently between different NP models and the SM.

3.3.2 Distributions of charged tau decay products

In figures 9 and 10, we give the products $n_0(\omega) \tilde{F}_{1,2}^d(\omega)$ (eqs. (3.8) and (3.9)) that can be obtained from the measurement of the double differential decay width $d\Gamma_d / (d\omega d \cos \theta_d)$

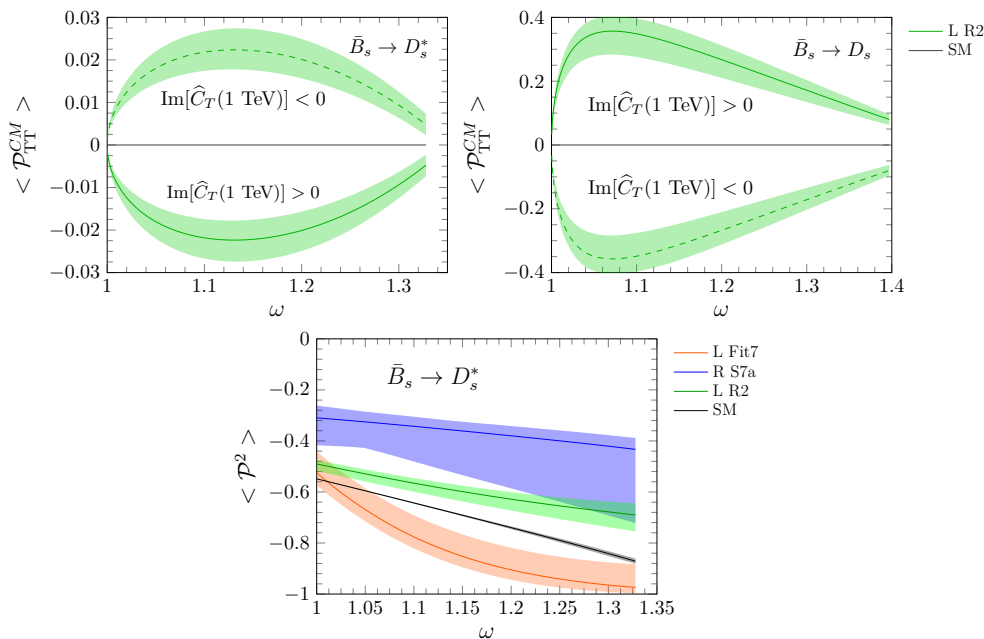


Figure 8. Upper panels: $\langle P_{TT}^{CM} \rangle(\omega)$ for the $\bar{B}_s \rightarrow D_s^*$ (left) and $\bar{B}_s \rightarrow D_s$ (right) decays evaluated with the $L R_2$ leptoquark model of ref. [66]. Bottom panel: comparison of the $\langle P^2 \rangle(\omega)$ distribution obtained in the SM and the NP extensions L Fit 7 [43], R S7a [68] and $L R_2$ [66].

corresponding to the $\bar{B}_s \rightarrow D_s^{(*)} \tau^- (\pi^- \nu_\tau, \rho^- \nu_\tau, \mu^- \bar{\nu}_\mu \nu_\tau) \bar{\nu}_\tau$ sequential decays.⁸ In most cases, with the main exception being the $\tau \rightarrow \rho \nu_\tau$ decay mode for the $\bar{B}_s \rightarrow D_s^*$ decay, the predictions from the L Fit 7 model are clearly distinguishable from the ones obtained in the SM and the other two NP scenarios. The SM and the latter two NP models give results that agree within errors.

A similar situation is seen in figure 11, where we display the normalized $[\mathcal{B}_d \Gamma_{\text{SL}}]^{-1} d\Gamma_d/d \cos \theta_d$ angular distribution for the $\bar{B}_s \rightarrow D_s^{(*)} \tau^- (\pi^- \nu_\tau, \rho^- \nu_\tau, \mu^- \bar{\nu}_\mu \nu_\tau) \bar{\nu}_\tau$ sequential decays. Again, with the exception of the ρ channel for the $\bar{B}_s \rightarrow D_s^*$ decay, we see that the L Fit 7 NP scenario of ref. [43] can be distinguished from the SM and the other two NP scenarios. This is most clearly seen for forward and backward angles of the pion and rho mesons from the hadronic τ -decay modes in the parent $\bar{B}_s \rightarrow D_s$ semileptonic decay. As for the R S7a scenario of ref. [68] and $L R_2$ Fit of ref. [66], their corresponding distributions are compatible with the SM and among themselves within errors. In fact, for the $L R_2$ model, the central values are very close to the SM ones. These behaviors derive from the ones seen for $\tilde{F}_{12}^d(\omega)$ in figures 9 and 10 and they are also seen in the corresponding $\tilde{F}_{1,2}^d$ coefficients that we give in tables 4 and 5 for the leptonic and two hadronic τ -decay channels, respectively. These latter coefficients are obtained after integrating over ω the $\tilde{F}_{1,2}^d(\omega)$ functions, as indicated in eq. (3.10), and depend on the tau-decay mode. For L Fit 7, we generally find that one coefficient, or both, is always very different from SM and other NP model values. For the

⁸The spin analyzing power makes the pion tau-decay mode a better candidate than the leptonic or rho modes for the extraction of information on the spin and spin-angular asymmetries (see discussion of eq. (2.11) of ref. [50]).

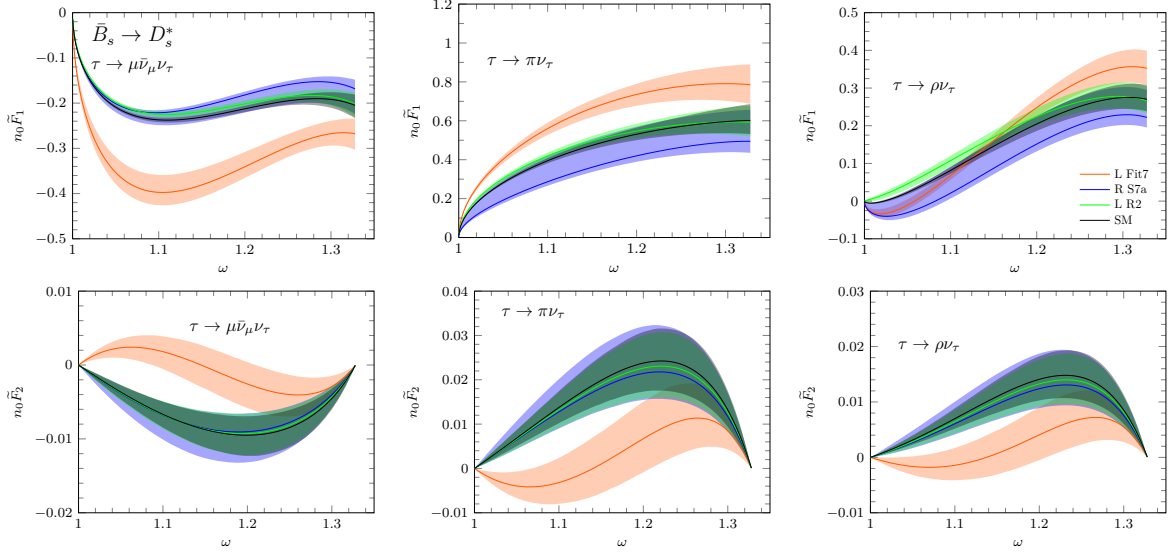


Figure 9. Distributions $[n_0\tilde{F}_1^d](\omega)$ and $[n_0\tilde{F}_2^d](\omega)$ obtained from $d\Gamma_d/(d\omega d\cos\theta_d)$ (eq. (3.7)) for the tau hadronic and leptonic $\bar{B}_s \rightarrow D_s^* \tau^-(\pi^-\nu_\tau, \rho^-\nu_\tau, \mu^-\bar{\nu}_\mu\nu_\tau)\bar{\nu}_\tau$ sequential decays.

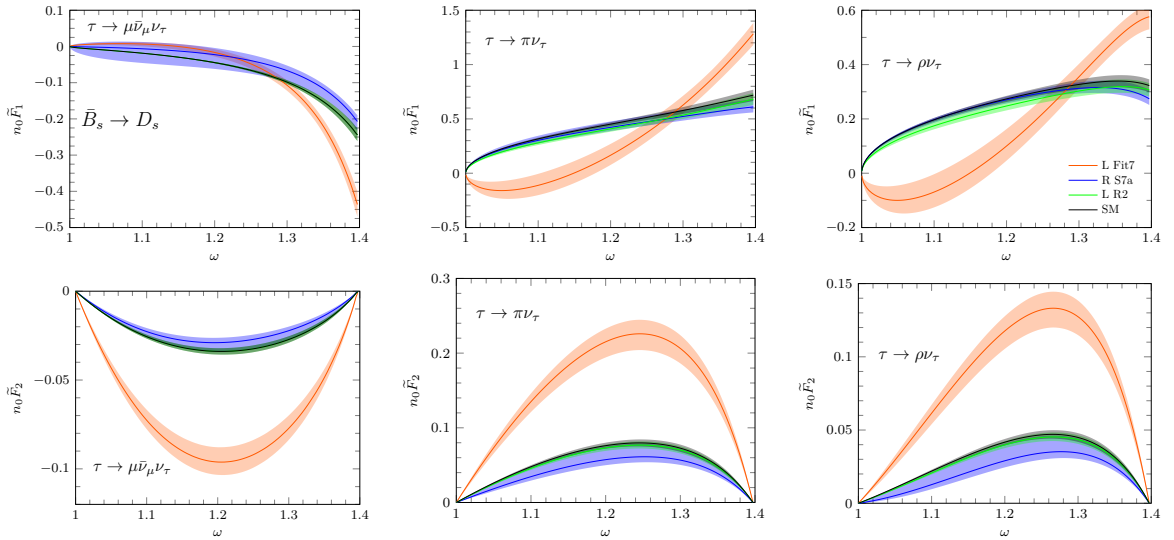


Figure 10. Same as figure 9 for the $\bar{B}_s \rightarrow D_s \tau^-(\pi^-\nu_\tau, \rho^-\nu_\tau, \mu^-\bar{\nu}_\mu\nu_\tau)\bar{\nu}_\tau$ sequential decays.

R S7a scenario, they are compatible with SM, within errors, and they are very close to the SM ones in the L R_2 case.

Finally, in figure 12, we present the results for the dimensionless distribution

$$\hat{F}_0^d(E_d) = \frac{m_\tau}{2\mathcal{B}_d\Gamma_{\text{SL}}} \frac{d\Gamma_d}{dE_d}, \quad (3.13)$$

which contains all the relevant information on the $d\Gamma_d/dE_d$ energy differential decay width. For all three tau-decay channels considered. It is normalized as

$$\frac{1}{m_\tau} \int_{E_d^{\text{min}}}^{E_d^{\text{max}}} dE_d \hat{F}_0^d(E_d) = \frac{1}{2}, \quad (3.14)$$

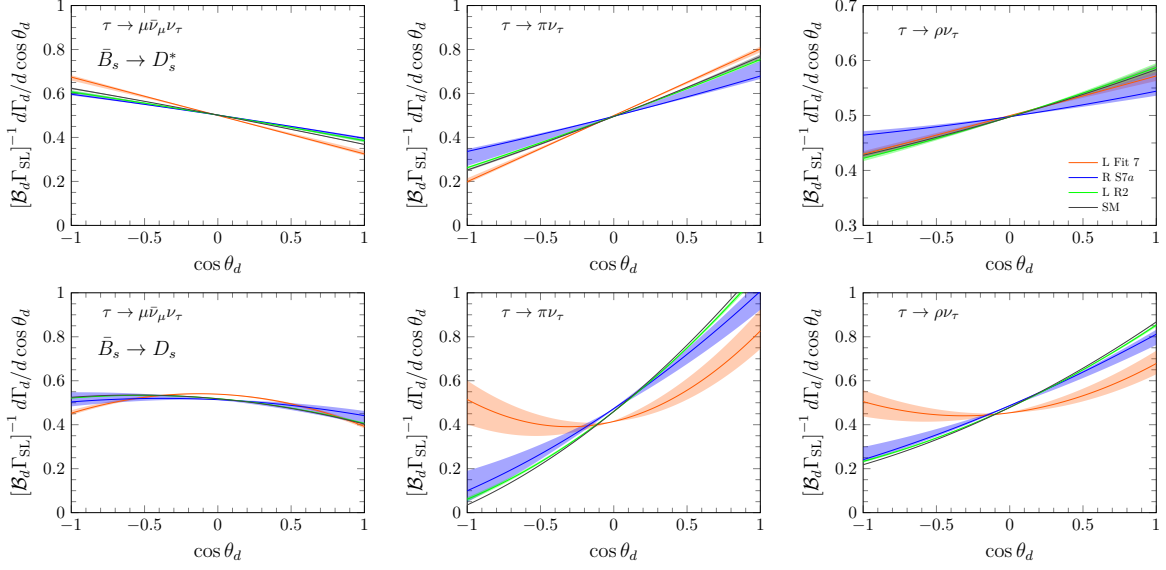


Figure 11. The ω -integrated $d\Gamma_d/d\cos\theta_d$ distributions for the $\bar{B}_s \rightarrow D_s^* \tau^- (\pi^- \nu_\tau, \rho^- \nu_\tau, \mu^- \bar{\nu}_\mu \nu_\tau) \bar{\nu}_\tau$ (top) and $\bar{B}_s \rightarrow D_s \tau^- (\pi^- \nu_\tau, \rho^- \nu_\tau, \mu^- \bar{\nu}_\mu \nu_\tau) \bar{\nu}_\tau$ (bottom) sequential decays. Units of $[\mathcal{B}_d \Gamma_{\text{SL}}]^{-1}$.

		\hat{F}_1^μ	\hat{F}_2^μ
$\bar{B}_s \rightarrow D_s$	SM	$-0.0608^{+0.0006}_{-0.0005}$	-0.0360 ± 0.0006
	L fit 7	$-0.030^{+0.008}_{-0.011}$	$-0.0777^{+0.0021}_{-0.0005}$
	R fit S7a	$-0.03^{+0.02}_{-0.04}$	-0.028 ± 0.003
	L R_2	$-0.0579^{+0.0024}_{-0.0018}$	$-0.0368^{+0.0022}_{-0.0013}$
$\bar{B}_s \rightarrow D_s^*$	SM	$-0.128^{+0.003}_{-0.002}$	-0.0042 ± 0.0010
	L Fit 7	$-0.175^{+0.014}_{-0.008}$	-0.0001 ± 0.0011
	R S7a	$-0.100^{+0.005}_{-0.016}$	$-0.0036^{+0.0010}_{-0.0017}$
	L R_2	$-0.111^{+0.004}_{-0.007}$	-0.0038 ± 0.0010

Table 4. Predictions for the angular moments $\hat{F}_{1,2}^\mu$ for the $\bar{B}_s \rightarrow D_s^{(*)} \tau (\mu \bar{\nu}_\mu \nu_\tau) \bar{\nu}_\tau$ sequential decay evaluated in the SM and the same NP scenarios considered in table 3.

		\hat{F}_1^π	\hat{F}_2^π	\hat{F}_1^ρ	\hat{F}_2^ρ
$\bar{B}_s \rightarrow D_s$	SM	$0.5443^{+0.0013}_{-0.0015}$	0.0794 ± 0.0014	$0.3247^{+0.0007}_{-0.0008}$	0.0428 ± 0.0008
	L fit 7	$0.16^{+0.11}_{-0.08}$	$0.171^{+0.002}_{-0.007}$	$0.09^{+0.06}_{-0.05}$	$0.0918^{+0.0016}_{-0.0046}$
	R fit S7a	$0.45^{+0.05}_{-0.09}$	$0.053^{+0.012}_{-0.007}$	$0.285^{+0.015}_{-0.053}$	$0.026^{+0.008}_{-0.004}$
	L R_2	$0.519^{+0.006}_{-0.011}$	$0.080^{+0.003}_{-0.005}$	$0.310^{+0.003}_{-0.006}$	$0.0431^{+0.0013}_{-0.0024}$
$\bar{B}_s \rightarrow D_s^*$	SM	0.258 ± 0.006	$0.010^{+0.003}_{-0.002}$	0.078 ± 0.007	0.0055 ± 0.0014
	L fit 7	$0.302^{+0.009}_{-0.016}$	0.001 ± 0.003	$0.071^{+0.007}_{-0.006}$	0.0006 ± 0.0016
	R fit S7a	$0.171^{+0.067}_{-0.012}$	$0.008^{+0.004}_{-0.002}$	$0.040^{+0.035}_{-0.007}$	$0.0042^{+0.0024}_{-0.0012}$
	L R_2	0.246 ± 0.007	$0.009^{+0.003}_{-0.002}$	$0.083^{+0.006}_{-0.007}$	0.0047 ± 0.0014

Table 5. Predictions for the angular moments $\hat{F}_{1,2}^{\pi,\rho}$ for the $\bar{B}_s \rightarrow D_s^{(*)} \tau (\pi \nu_\tau, \rho \nu_\tau) \bar{\nu}_\tau$ sequential decays evaluated in the SM and the same NP scenarios considered in table 3.

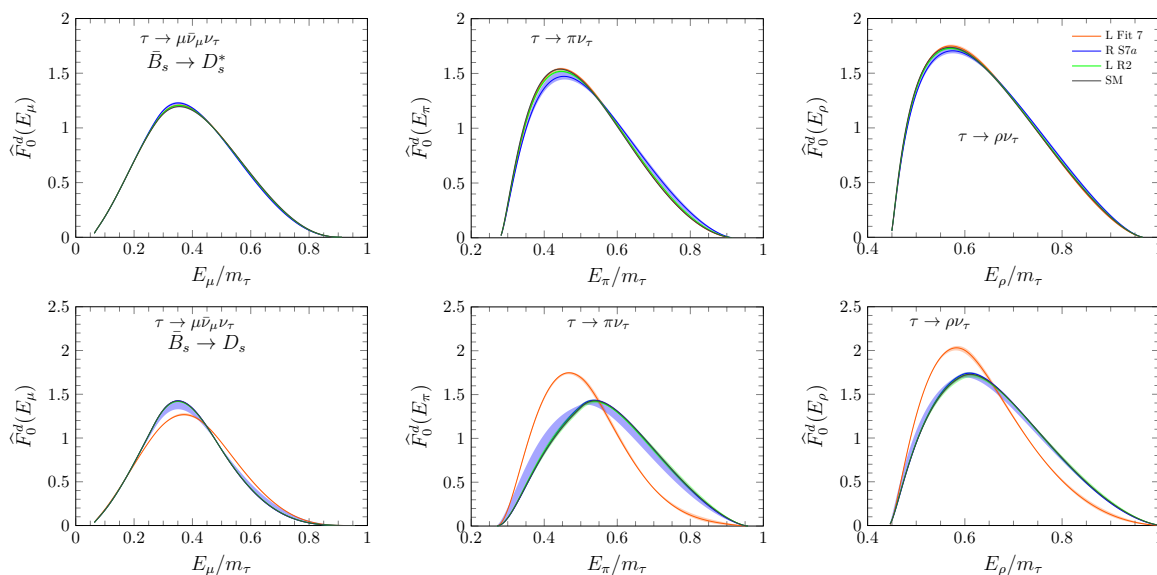


Figure 12. \widehat{F}_0^d distribution (eq. (3.13)) for the $\bar{B}_s \rightarrow D_s^{(*)} \tau^- (\pi^- \nu_\tau, \rho^- \nu_\tau, \mu^- \bar{\nu}_\mu \nu_\tau) \bar{\nu}_\tau$ sequential decays.

but its energy dependence is still affected by the CM τ longitudinal polarization $\langle P_L^{\text{CM}} \rangle(\omega)$. However, as seen in figure 12, for the $\bar{B}_s \rightarrow D_s^*$ parent decay, all NP scenarios considered are compatible with SM predictions, and among themselves, within uncertainties, while for the $\bar{B}_s \rightarrow D_s$, the distribution obtained from the L Fit 7 NP model of ref. [43] can be distinguished from all other predictions.

4 Summary

We have used the results of the lattice evaluation of the SM form factors for the $\bar{B}_s \rightarrow D_s$ [32] and the SM and tensor form factors for the $\bar{B}_s \rightarrow D_s^*$ [34] semileptonic decays, together with their NLO HQET expansions in ref. [35], to obtain in addition the scalar and pseudoscalar form factors of both transitions and the $\bar{B}_s \rightarrow D_s$ tensor matrix element, all of them also needed for an analysis of NP effects on both semileptonic decays. We have compared results evaluated within the SM and three different NP extensions that have been previously used in the study of other CC $b \rightarrow c$ transitions. We find effects similar to those obtained for the SU(3)-analogue $\bar{B} \rightarrow D^{(*)}$ decays. We have evaluated the corresponding \mathcal{R}_{D_s} and $\mathcal{R}_{D_s^*}$ ratios which, as in the $\bar{B} \rightarrow D^{(*)}$ case, should be the easiest LFUV observable to measure. We have also analyzed the role that different tau asymmetries in the $\bar{B}_s \rightarrow D_s^{(*)} \tau^- \bar{\nu}_\tau$ decay could play, not only in establishing the existence of NP, but also in distinguishing between different NP extensions of the SM. We have studied partially integrated angular and energy distributions of the charged particle produced in the subsequent $\tau^- \rightarrow \pi^- \nu_\tau, \rho^- \nu_\tau, e^- (\mu^-) \bar{\nu}_{e(\mu)} \nu_\tau$ decays. The latter differential decay widths have a better statistics than the asymmetries themselves and they could also help in establishing the presence of NP beyond the SM.

If NP is responsible for LFUV it should show up in $\bar{B}_s \rightarrow D_s^{(*)}$ semileptonic decays at the same level as for the $\bar{B} \rightarrow D^{(*)}$ ones. The analysis of this transition, as well of other CC

	a_0^0	a_1^0	a_2^0	a_0^+	a_1^+
	0.674 ± 0.009	-0.238 ± 0.218	-0.13 ± 1.61	0.764 ± 0.018	-3.04 ± 0.43
a_0^0	1.00	0.117	-0.074	0.567	-0.011
a_1^0		1.00	-0.062	0.421	-0.030
a_2^0			1.00	-0.145	0.229
a_0^+				1.00	-0.726
a_1^+					1.00

Table 6. Central values and errors (first row) of the $a_i^{0,+}$ coefficients of the new $f_{+,0}$ parametrization introduced in eq. (2.6) and their corresponding correlation matrix. Note that a_2^+ is fixed through the condition $f_0(0) = f_+(0)$.

	h_{A_1}	h_{A_2}	h_{A_3}	h_V
a_0	0.907 ± 0.010	-0.333 ± 0.129	1.14 ± 0.13	1.25 ± 0.04
a_1	-1.01 ± 0.09	-0.066 ± 0.639	-0.649 ± 0.539	-1.51 ± 0.26
a_2	0.379 ± 0.435	0.065 ± 0.948	-0.200 ± 0.853	0.507 ± 0.752
a_3	0.275 ± 0.817	0.007 ± 0.989	-0.101 ± 0.961	0.373 ± 0.938

Table 7. Central values and errors of the a_i^F coefficients of the new parametrization ($(\omega - 1)$ expansion) introduced in eq. (2.9) for the $h_{A_1}, h_{A_2}, h_{A_3}$ and h_V form factors.

$b \rightarrow c$ mediated decays, could then help in establishing or ruling out LFUV.

Acknowledgments

N.P. thanks Physics and Astronomy at the University of Southampton for hospitality during the making of this work and a Generalitat Valenciana grant CIBAFP/2021/32. This research has been supported by the Spanish Ministerio de Ciencia e Innovación (MICINN) and the European Regional Development Fund (ERDF) under contracts PID2020-112777GB-I00 and PID2019-105439GB-C22, the EU STRONG-2020 project under the program H2020-INFRAIA-2018-1, grant agreement no. 824093 and by Generalitat Valenciana under contract PROMETEO/2020/023.

A Mean values and covariance matrices of the a_i^F coefficients in eqs. (2.6), (2.7) and (2.9)

As discussed in the main text, we have changed the parametrizations in refs. [32, 34] and adopted new ones in order to facilitate the fitting of the form factors to their HQSS expressions. Statistical details of the new coefficients are collected here in tables 6–13. For each entry in the tables below, we provide three significant digits but neglect order 10^{-5} or smaller.

Open Access. This article is distributed under the terms of the Creative Commons Attribution License ([CC-BY4.0](https://creativecommons.org/licenses/by/4.0/)), which permits any use, distribution and reproduction in any medium, provided the original author(s) and source are credited.

	h_{T_1}	h_{T_2}	h_{T_3}
a_0	0.933 ± 0.015	-0.152 ± 0.045	-0.027 ± 0.149
a_1	-1.09 ± 0.10	0.231 ± 0.286	0.106 ± 0.661
a_2	0.512 ± 0.473	0.449 ± 0.892	0.019 ± 0.939
a_3	0.138 ± 0.858	0.244 ± 0.979	0.005 ± 0.988

Table 8. Central values and errors of the a_i^F coefficients of the new parametrization $((\omega - 1)$ -expansion) introduced in eq. (2.9) for the h_{T_1}, h_{T_2} and h_{T_3} form factors.

	$a_0^{A_1}$	$a_1^{A_1}$	$a_2^{A_1}$	$a_3^{A_1}$	$a_0^{A_2}$	$a_1^{A_2}$	$a_2^{A_2}$	$a_3^{A_2}$	$a_0^{A_3}$	$a_1^{A_3}$	$a_2^{A_3}$	$a_3^{A_3}$
$a_0^{A_1}$	1.00	-0.160	0.0523	-0.0128	0.0144	-0.0177	-0.0037	-0.0008	0.0469	-0.0055	0.0039	0.0041
$a_1^{A_1}$		1.00	-0.6252	0.2511	-0.2650	0.1381	0.0124	0.0011	0.3039	-0.1410	-0.0879	-0.0342
$a_2^{A_1}$			1.00	-0.7071	0.0971	-0.1797	-0.0297	-0.0108	-0.1326	0.2761	0.0374	-0.0025
$a_3^{A_1}$				1.00	0.0646	-0.0750	0.0113	0.0141	-0.0550	0.0006	0.1622	0.0921
$a_0^{A_2}$					1.00	-0.3542	-0.0309	-0.0108	-0.8365	0.4847	-0.0390	-0.0365
$a_1^{A_2}$						1.00	-0.2141	-0.0479	0.1783	-0.5943	0.0635	0.0510
$a_2^{A_2}$							1.00	-0.0478	0.0824	-0.0981	-0.1070	-0.0465
$a_3^{A_2}$								1.00	0.0310	-0.0212	-0.0592	-0.0289
$a_0^{A_3}$									1.00	-0.5695	0.1206	0.0622
$a_1^{A_3}$										1.00	-0.4675	-0.1211
$a_2^{A_3}$											1.00	-0.1682
$a_3^{A_3}$												1.00

Table 9. Correlation matrix for the $(w - 1)$ -expansion coefficients of the h_{A_1}, h_{A_2} and h_{A_3} form factors.

	a_0^V	a_1^V	a_2^V	a_3^V
a_0^V	1.00	-0.526	0.251	0.0672
a_1^V		1.00	-0.720	-0.0557
a_2^V			1.00	-0.307
a_3^V				1.00

Table 10. Correlation matrix for the $(w - 1)$ -expansion coefficients of the h_V form factor.

	$a_0^{A_1}$	$a_1^{A_1}$	$a_2^{A_1}$	$a_3^{A_1}$	$a_0^{A_2}$	$a_1^{A_2}$	$a_2^{A_2}$	$a_3^{A_2}$	$a_0^{A_3}$	$a_1^{A_3}$	$a_2^{A_3}$	$a_3^{A_3}$
a_0^V	0.0695	-0.0034	-0.0023	-0.0029	0.0187	-0.0044	-0.0054	-0.0024	-0.0022	0.0072	-0.0024	-0.0011
a_1^V	0.0151	0.0181	0.0034	-0.0045	0.0149	0.0137	0.0015	0.0003	-0.0120	0.0054	0.0023	0.0013
a_2^V	-0.0094	-0.0045	0.0107	0.0057	-0.0018	0.0137	0.0093	0.0041	-0.0043	-0.0021	0.0060	0.0031
a_3^V	-0.0032	-0.0022	0.0040	0.0028	-0.0017	0.0051	0.0038	0.0017	-0.0009	-0.0009	0.0023	0.0011

Table 11. Correlation matrix for the $(w - 1)$ -expansion coefficients of h_V and h_{A_1}, h_{A_2} and h_{A_3} form factors.

	$a_0^{T_1}$	$a_1^{T_1}$	$a_2^{T_1}$	$a_3^{T_1}$	$a_0^{T_2}$	$a_1^{T_2}$	$a_2^{T_2}$	$a_3^{T_2}$	$a_0^{T_3}$	$a_1^{T_3}$	$a_2^{T_3}$	$a_3^{T_3}$
$a_0^{T_1}$	1.00	-0.230	0.0740	-0.0056	0.0593	-0.0300	0.0044	0.0025	0.0252	-0.0101	0.0030	0.0027
$a_1^{T_1}$		1.00	-0.633	0.208	0.0328	0.0912	-0.0629	-0.0285	0.304	-0.154	-0.0689	-0.0272
$a_2^{T_1}$			1.00	-0.645	-0.0483	0.0569	0.112	0.0456	-0.136	0.293	0.0586	0.0134
$a_3^{T_1}$				1.00	0.0025	-0.0379	0.0511	0.0306	-0.0511	0.0546	0.0738	0.0389
$a_0^{T_2}$					1.00	-0.471	0.130	0.0347	0.0446	-0.0400	-0.0140	-0.0051
$a_1^{T_2}$						1.00	-0.589	-0.0819	0.0828	0.0552	0.0017	-0.0022
$a_2^{T_2}$							1.00	-0.0957	-0.0427	0.135	0.0491	0.0192
$a_3^{T_2}$								1.00	-0.0212	0.0615	0.0239	0.0097
$a_0^{T_3}$									1.00	-0.573	0.0128	0.0227
$a_1^{T_3}$										1.00	-0.336	-0.111
$a_2^{T_3}$											1.00	-0.0548
$a_3^{T_3}$												1.00

Table 12. Correlation matrix for the $(w - 1)$ -expansion coefficients of the h_{T_1} , h_{T_2} and h_{T_3} form factors.

	$a_0^{A_1}$	$a_1^{A_1}$	$a_2^{A_1}$	$a_3^{A_1}$	$a_0^{A_2}$	$a_1^{A_2}$	$a_2^{A_2}$	$a_3^{A_2}$	$a_0^{A_3}$	$a_1^{A_3}$	$a_2^{A_3}$	$a_3^{A_3}$
$a_0^{A_1}$	0.289	-0.0368	0.0078	-0.0004	-0.0098	-0.0112	-0.0003	-0.0004	0.0005	-0.0001	0.0018	0.0010
$a_1^{A_1}$	-0.0123	0.210	-0.0882	-0.0290	0.0170	0.0175	0.0028	0.0022	0.0534	-0.0048	-0.0028	-0.0015
$a_2^{A_1}$	-0.0018	-0.0940	0.185	-0.0099	-0.0121	0.0043	0.0040	0.0016	-0.0047	0.0373	0.0256	0.0126
$a_3^{A_1}$	-0.0016	-0.0243	-0.0214	0.0842	0.0008	0.0083	-0.0120	-0.0075	-0.0006	0.0219	-0.0178	-0.0116
$a_0^{A_2}$	0.0095	-0.0794	0.0079	0.0066	0.0053	-0.0095	-0.0054	-0.0034	-0.189	0.0284	0.0124	0.0052
$a_1^{A_2}$	0.0000	0.0200	-0.0534	-0.0228	-0.0012	-0.0048	0.0113	0.0059	-0.0112	-0.110	-0.0261	-0.0079
$a_2^{A_2}$	-0.0019	-0.0079	0.0034	0.0051	-0.0027	-0.0012	0.0042	0.0020	0.0102	-0.0312	-0.0100	-0.0037
$a_3^{A_2}$	-0.0009	-0.0050	0.0040	0.0040	-0.0013	-0.0003	0.0016	0.0007	0.0052	-0.0111	-0.0041	-0.0016
$a_0^{A_3}$	0.0179	0.0881	-0.0170	-0.0105	0.0023	0.0100	0.0052	0.0034	0.205	-0.0254	-0.0119	-0.0050
$a_1^{A_3}$	0.0004	-0.0160	0.0690	0.0316	0.0011	0.0125	-0.0105	-0.0061	-0.0541	0.119	0.0260	0.0074
$a_2^{A_3}$	-0.0051	-0.0287	0.0593	0.0050	-0.0047	0.0051	-0.0023	-0.0018	-0.0031	0.0178	0.0131	0.0063
$a_3^{A_3}$	-0.0020	-0.0138	0.0270	0.0007	-0.0026	0.0020	-0.0005	-0.0005	-0.0002	0.0029	0.0054	0.0029
a_0^V	0.0694	-0.0022	-0.0003	-0.0009	0.0304	0.0021	-0.0006	-0.0002	0.0043	0.0132	0.0036	0.0013
a_1^V	0.0041	0.0141	0.0027	-0.0028	-0.0012	0.0127	-0.0025	-0.0014	-0.0106	0.0030	0.0033	0.0016
a_2^V	-0.0075	-0.0023	0.0091	0.0049	-0.0039	0.0018	0.0062	0.0026	0.0032	-0.0043	-0.0029	-0.0014
a_3^V	-0.0026	-0.0012	0.0034	0.0025	-0.0015	0.0005	0.0028	0.0012	0.0018	-0.0019	-0.0015	-0.0008

Table 13. Correlation matrix for the $(w - 1)$ -expansion between the h_{T_1} , h_{T_2} and h_{T_3} and the h_{A_1} , h_{A_2} , h_{A_3} and h_V coefficients.

References

- [1] BABAR collaboration, *Evidence for an excess of $\bar{B} \rightarrow D^{(*)}\tau^-\bar{\nu}_\tau$ decays*, *Phys. Rev. Lett.* **109** (2012) 101802 [[arXiv:1205.5442](#)] [[INSPIRE](#)].
- [2] BABAR collaboration, *Measurement of an Excess of $\bar{B} \rightarrow D^{(*)}\tau^-\bar{\nu}_\tau$ Decays and Implications for Charged Higgs Bosons*, *Phys. Rev. D* **88** (2013) 072012 [[arXiv:1303.0571](#)] [[INSPIRE](#)].
- [3] BELLE collaboration, *Measurement of the branching ratio of $\bar{B} \rightarrow D^{(*)}\tau^-\bar{\nu}_\tau$ relative to $\bar{B} \rightarrow D^{(*)}\ell^-\bar{\nu}_\ell$ decays with hadronic tagging at Belle*, *Phys. Rev. D* **92** (2015) 072014 [[arXiv:1507.03233](#)] [[INSPIRE](#)].

- [4] BELLE collaboration, *Measurement of the branching ratio of $\bar{B}^0 \rightarrow D^{*+}\tau^-\bar{\nu}_\tau$ relative to $\bar{B}^0 \rightarrow D^{*+}\ell^-\bar{\nu}_\ell$ decays with a semileptonic tagging method*, *Phys. Rev. D* **94** (2016) 072007 [[arXiv:1607.07923](#)] [[INSPIRE](#)].
- [5] BELLE collaboration, *Measurement of the τ lepton polarization and $R(D^*)$ in the decay $\bar{B} \rightarrow D^*\tau^-\bar{\nu}_\tau$* , *Phys. Rev. Lett.* **118** (2017) 211801 [[arXiv:1612.00529](#)] [[INSPIRE](#)].
- [6] BELLE collaboration, *Measurement of $\mathcal{R}(D)$ and $\mathcal{R}(D^*)$ with a semileptonic tagging method*, *Phys. Rev. Lett.* **124** (2020) 161803 [[arXiv:1910.05864](#)] [[INSPIRE](#)].
- [7] LHCb collaboration, *Measurement of the ratio of branching fractions $\mathcal{B}(\bar{B}^0 \rightarrow D^{*+}\tau^-\bar{\nu}_\tau)/\mathcal{B}(\bar{B}^0 \rightarrow D^{*+}\mu^-\bar{\nu}_\mu)$* , *Phys. Rev. Lett.* **115** (2015) 111803 [Erratum *ibid.* **115** (2015) 159901] [[arXiv:1506.08614](#)] [[INSPIRE](#)].
- [8] LHCb collaboration, *Measurement of the ratio of the $B^0 \rightarrow D^{*-}\tau^+\nu_\tau$ and $B^0 \rightarrow D^{*-}\mu^+\nu_\mu$ branching fractions using three-prong τ -lepton decays*, *Phys. Rev. Lett.* **120** (2018) 171802 [[arXiv:1708.08856](#)] [[INSPIRE](#)].
- [9] LHCb collaboration, *Test of Lepton Flavor Universality by the measurement of the $B^0 \rightarrow D^{*-}\tau^+\nu_\tau$ branching fraction using three-prong τ decays*, *Phys. Rev. D* **97** (2018) 072013 [[arXiv:1711.02505](#)] [[INSPIRE](#)].
- [10] LHCb collaboration, *Measurement of the ratios of branching fractions $\mathcal{R}(D^*)$ and $\mathcal{R}(D^0)$* , *Phys. Rev. Lett.* **131** (2023) 111802 [[arXiv:2302.02886](#)] [[INSPIRE](#)].
- [11] HFLAV collaboration, *Averages of b -hadron, c -hadron, and τ -lepton properties as of 2018*, *Eur. Phys. J. C* **81** (2021) 226 [[arXiv:1909.12524](#)] [[INSPIRE](#)].
- [12] R. Puthumanai, *Measurement of $R(D^*)$ with hadronic τ^+ decays at $\sqrt{s} = 13$ TeV by the LHCb collaboration*, CERN LHC Seminar, March 21 (2023), <https://cds.cern.ch/record/2862148>.
- [13] LHCb collaboration, *Measurement of the ratio of branching fractions $\mathcal{B}(B_c^+ \rightarrow J/\psi\tau^+\nu_\tau)/\mathcal{B}(B_c^+ \rightarrow J/\psi\mu^+\nu_\mu)$* , *Phys. Rev. Lett.* **120** (2018) 121801 [[arXiv:1711.05623](#)] [[INSPIRE](#)].
- [14] A.Y. Anisimov, I.M. Narodetsky, C. Semay and B. Silvestre-Brac, *The B_c meson lifetime in the light front constituent quark model*, *Phys. Lett. B* **452** (1999) 129 [[hep-ph/9812514](#)] [[INSPIRE](#)].
- [15] M.A. Ivanov, J.G. Korner and P. Santorelli, *Exclusive semileptonic and nonleptonic decays of the B_c meson*, *Phys. Rev. D* **73** (2006) 054024 [[hep-ph/0602050](#)] [[INSPIRE](#)].
- [16] E. Hernandez, J. Nieves and J.M. Verde-Velasco, *Study of exclusive semileptonic and non-leptonic decays of B_c - in a nonrelativistic quark model*, *Phys. Rev. D* **74** (2006) 074008 [[hep-ph/0607150](#)] [[INSPIRE](#)].
- [17] T. Huang and F. Zuo, *Semileptonic B_c decays and charmonium distribution amplitude*, *Eur. Phys. J. C* **51** (2007) 833 [[hep-ph/0702147](#)] [[INSPIRE](#)].
- [18] W. Wang, Y.-L. Shen and C.-D. Lu, *Covariant Light-Front Approach for $B(c)$ transition form factors*, *Phys. Rev. D* **79** (2009) 054012 [[arXiv:0811.3748](#)] [[INSPIRE](#)].
- [19] W.-F. Wang, Y.-Y. Fan and Z.-J. Xiao, *Semileptonic decays $B_c \rightarrow (\eta_c, J/\Psi)l\nu$ in the perturbative QCD approach*, *Chin. Phys. C* **37** (2013) 093102 [[arXiv:1212.5903](#)] [[INSPIRE](#)].
- [20] R. Watanabe, *New Physics effect on $B_c \rightarrow J/\psi\tau\bar{\nu}$ in relation to the $R_{D^{(*)}}$ anomaly*, *Phys. Lett. B* **776** (2018) 5 [[arXiv:1709.08644](#)] [[INSPIRE](#)].
- [21] A. Issadykov and M.A. Ivanov, *The decays $B_c \rightarrow J/\psi + \bar{l}\nu_\ell$ and $B_c \rightarrow J/\psi + \pi(K)$ in covariant confined quark model*, *Phys. Lett. B* **783** (2018) 178 [[arXiv:1804.00472](#)] [[INSPIRE](#)].

- [22] C.-T. Tran, M.A. Ivanov, J.G. Körner and P. Santorelli, *Implications of new physics in the decays $B_c \rightarrow (J/\psi, \eta_c)\tau\nu$* , *Phys. Rev. D* **97** (2018) 054014 [[arXiv:1801.06927](#)] [[INSPIRE](#)].
- [23] X.-Q. Hu, S.-P. Jin and Z.-J. Xiao, *Semileptonic decays $B_c \rightarrow (\eta_c, J/\psi)l\bar{\nu}_l$ in the “PQCD + Lattice” approach*, *Chin. Phys. C* **44** (2020) 023104 [[arXiv:1904.07530](#)] [[INSPIRE](#)].
- [24] D. Leljak, B. Melic and M. Patra, *On lepton flavour universality in semileptonic $B_c \rightarrow \eta_c, J/\psi$ decays*, *JHEP* **05** (2019) 094 [[arXiv:1901.08368](#)] [[INSPIRE](#)].
- [25] K. Azizi, Y. Sarac and H. Sundu, *Lepton flavor universality violation in semileptonic tree level weak transitions*, *Phys. Rev. D* **99** (2019) 113004 [[arXiv:1904.08267](#)] [[INSPIRE](#)].
- [26] W. Wang and R. Zhu, *Model independent investigation of the $R_{J/\psi, \eta_c}$ and ratios of decay widths of semileptonic B_c decays into a P-wave charmonium*, *Int. J. Mod. Phys. A* **34** (2019) 1950195 [[arXiv:1808.10830](#)] [[INSPIRE](#)].
- [27] LHCb collaboration, *Observation of the decay $\Lambda_b^0 \rightarrow \Lambda_c^+ \tau^- \bar{\nu}_\tau$* , *Phys. Rev. Lett.* **128** (2022) 191803 [[arXiv:2201.03497](#)] [[INSPIRE](#)].
- [28] W. Detmold, C. Lehner and S. Meinel, *$\Lambda_b \rightarrow p\ell^- \bar{\nu}_\ell$ and $\Lambda_b \rightarrow \Lambda_c \ell^- \bar{\nu}_\ell$ form factors from lattice QCD with relativistic heavy quarks*, *Phys. Rev. D* **92** (2015) 034503 [[arXiv:1503.01421](#)] [[INSPIRE](#)].
- [29] Marco Pappagallo (LHCb deputy physics coordinator), private communication.
- [30] LHCb collaboration, *Test of lepton flavor universality using $B^0 \rightarrow D^{*+} \tau + \nu \tau$ decays with hadronic τ channels*, *Phys. Rev. D* **108** (2023) 012018 [[arXiv:2305.01463](#)] [[INSPIRE](#)].
- [31] HFLAV collaboration, *Averages of b-hadron, c-hadron, and τ -lepton properties as of 2021*, *Phys. Rev. D* **107** (2023) 052008 [[arXiv:2206.07501](#)] [[INSPIRE](#)].
- [32] E. McLean, C.T.H. Davies, J. Koponen and A.T. Lytle, *$B_s \rightarrow D_s \ell \nu$ Form Factors for the full q^2 range from Lattice QCD with non-perturbatively normalized currents*, *Phys. Rev. D* **101** (2020) 074513 [[arXiv:1906.00701](#)] [[INSPIRE](#)].
- [33] HPQCD collaboration, *$B_s \rightarrow D_s^*$ form factors for the full q^2 range from lattice QCD*, *Phys. Rev. D* **105** (2022) 094506 [[arXiv:2105.11433](#)] [[INSPIRE](#)].
- [34] J. Harrison and C.T.H. Davies, *$B \rightarrow D^*$ vector, axial-vector and tensor form factors for the full q^2 range from lattice QCD*, [arXiv:2304.03137](#) [[INSPIRE](#)].
- [35] F.U. Bernlochner, Z. Ligeti, M. Papucci and D.J. Robinson, *Combined analysis of semileptonic B decays to D and D^* : $R(D^{(*)})$, $|V_{cb}|$, and new physics*, *Phys. Rev. D* **95** (2017) 115008 [*Erratum ibid.* **97** (2018) 059902] [[arXiv:1703.05330](#)] [[INSPIRE](#)].
- [36] F.U. Bernlochner et al., *Constrained second-order power corrections in HQET: $R(D^{(*)})$, $|V_{cb}|$, and new physics*, *Phys. Rev. D* **106** (2022) 096015 [[arXiv:2206.11281](#)] [[INSPIRE](#)].
- [37] M. Bordone, M. Jung and D. van Dyk, *Theory determination of $\bar{B} \rightarrow D^{(*)} \ell^- \bar{\nu}$ form factors at $\mathcal{O}(1/m_c^2)$* , *Eur. Phys. J. C* **80** (2020) 74 [[arXiv:1908.09398](#)] [[INSPIRE](#)].
- [38] M. Bordone, N. Gubernari, D. van Dyk and M. Jung, *Heavy-Quark expansion for $\bar{B}_s \rightarrow D_s^{(*)}$ form factors and unitarity bounds beyond the $SU(3)_F$ limit*, *Eur. Phys. J. C* **80** (2020) 347 [[arXiv:1912.09335](#)] [[INSPIRE](#)].
- [39] R. Dutta and N. Rajeev, *Signature of lepton flavor universality violation in $B_s \rightarrow D_s \tau \nu$ semileptonic decays*, *Phys. Rev. D* **97** (2018) 095045 [[arXiv:1803.03038](#)] [[INSPIRE](#)].
- [40] N. Das and R. Dutta, *New physics footprints in the angular distribution of $B_s \rightarrow D_s^* (\rightarrow D_s \gamma, D_s \pi) \tau \nu$ decays*, *Phys. Rev. D* **105** (2022) 055027 [[arXiv:2110.05526](#)] [[INSPIRE](#)].

- [41] C.J. Monahan et al., $B_s \rightarrow D_s \ell \nu$ Form Factors and the Fragmentation Fraction Ratio f_s/f_d , *Phys. Rev. D* **95** (2017) 114506 [[arXiv:1703.09728](#)] [[INSPIRE](#)].
- [42] M.E. Luke, *Effects of subleading operators in the heavy quark effective theory*, *Phys. Lett. B* **252** (1990) 447 [[INSPIRE](#)].
- [43] C. Murgui, A. Peñuelas, M. Jung and A. Pich, *Global fit to $b \rightarrow c \tau \nu$ transitions*, *JHEP* **09** (2019) 103 [[arXiv:1904.09311](#)] [[INSPIRE](#)].
- [44] M. Jung and D.M. Straub, *Constraining new physics in $b \rightarrow c \ell \nu$ transitions*, *JHEP* **01** (2019) 009 [[arXiv:1801.01112](#)] [[INSPIRE](#)].
- [45] N. Penalva, E. Hernández and J. Nieves, *New physics and the tau polarization vector in $b \rightarrow c \tau \bar{\nu}_\tau$ decays*, *JHEP* **06** (2021) 118 [[arXiv:2103.01857](#)] [[INSPIRE](#)].
- [46] N. Penalva, E. Hernández and J. Nieves, *The role of right-handed neutrinos in $b \rightarrow c_\tau$ ($\pi \nu_\tau, \rho \nu_\tau, \mu \bar{\nu}_\mu \nu_\tau$) $\bar{\nu}_\tau$ from visible final-state kinematics*, *JHEP* **10** (2021) 122 [[arXiv:2107.13406](#)] [[INSPIRE](#)].
- [47] R. Alonso, A. Kobach and J. Martin Camalich, *New physics in the kinematic distributions of $\bar{B} \rightarrow D^{(*)} \tau^- (\rightarrow \ell^- \bar{\nu}_\ell \nu_\tau) \bar{\nu}_\tau$* , *Phys. Rev. D* **94** (2016) 094021 [[arXiv:1602.07671](#)] [[INSPIRE](#)].
- [48] R. Alonso, J. Martin Camalich and S. Westhoff, *Tau properties in $B \rightarrow D \tau \nu$ from visible final-state kinematics*, *Phys. Rev. D* **95** (2017) 093006 [[arXiv:1702.02773](#)] [[INSPIRE](#)].
- [49] P. Asadi et al., *Complete framework for tau polarimetry in $B \rightarrow D^{(*)} \tau \nu$ decays*, *Phys. Rev. D* **102** (2020) 095028 [[arXiv:2006.16416](#)] [[INSPIRE](#)].
- [50] N. Penalva et al., *Visible energy and angular distributions of the charged particle from the τ –decay in $b \rightarrow c \tau (\mu \bar{\nu}_\mu \nu_\tau, \pi \nu_\tau, \rho \nu_\tau) \bar{\nu}_\tau$ reactions*, *JHEP* **04** (2022) 026 [Erratum *ibid.* **03** (2023) 011] [[arXiv:2201.05537](#)] [[INSPIRE](#)].
- [51] N. Penalva, E. Hernández and J. Nieves, *Hadron and lepton tensors in semileptonic decays including new physics*, *Phys. Rev. D* **101** (2020) 113004 [[arXiv:2004.08253](#)] [[INSPIRE](#)].
- [52] N. Penalva, E. Hernández and J. Nieves, $\bar{B}_c \rightarrow \eta_c, \bar{B}_c \rightarrow J/\psi$ and $\bar{B} \rightarrow D^{(*)}$ semileptonic decays including new physics, *Phys. Rev. D* **102** (2020) 096016 [[arXiv:2007.12590](#)] [[INSPIRE](#)].
- [53] S. Fajfer, J.F. Kamenik and I. Nisandzic, *On the $B \rightarrow D^* \tau \bar{\nu}_\tau$ Sensitivity to New Physics*, *Phys. Rev. D* **85** (2012) 094025 [[arXiv:1203.2654](#)] [[INSPIRE](#)].
- [54] BELLE collaboration, *Measurement of the D^{*-} polarization in the decay $B^0 \rightarrow D^{*-} \tau^+ \nu_\tau$* , in the proceedings of the *10th International Workshop on the CKM Unitarity Triangle*, Heidelberg, Germany, September 17–21 (2018) [[arXiv:1903.03102](#)] [[INSPIRE](#)].
- [55] R. Alonso, B. Grinstein and J. Martin Camalich, *Lifetime of B_c^- Constrains Explanations for Anomalies in $B \rightarrow D^{(*)} \tau \nu$* , *Phys. Rev. Lett.* **118** (2017) 081802 [[arXiv:1611.06676](#)] [[INSPIRE](#)].
- [56] U. Nierste, S. Trine and S. Westhoff, *Charged-Higgs effects in a new $B \rightarrow D$ tau nu differential decay distribution*, *Phys. Rev. D* **78** (2008) 015006 [[arXiv:0801.4938](#)] [[INSPIRE](#)].
- [57] M. Tanaka and R. Watanabe, *New physics in the weak interaction of $\bar{B} \rightarrow D^{(*)} \tau \bar{\nu}$* , *Phys. Rev. D* **87** (2013) 034028 [[arXiv:1212.1878](#)] [[INSPIRE](#)].
- [58] M. Duraisamy and A. Datta, *The Full $B \rightarrow D^* \tau^- \bar{\nu}_\tau$ Angular Distribution and CP violating Triple Products*, *JHEP* **09** (2013) 059 [[arXiv:1302.7031](#)] [[INSPIRE](#)].
- [59] M. Duraisamy, P. Sharma and A. Datta, *Azimuthal $B \rightarrow D^* \tau^- \bar{\nu}_\tau$ angular distribution with tensor operators*, *Phys. Rev. D* **90** (2014) 074013 [[arXiv:1405.3719](#)] [[INSPIRE](#)].

- [60] D. Becirevic, S. Fajfer, I. Nisandzic and A. Tayduganov, *Angular distributions of $\bar{B} \rightarrow D^{(*)} \ell \bar{\nu}_\ell$ decays and search of New Physics*, *Nucl. Phys. B* **946** (2019) 114707 [[arXiv:1602.03030](#)] [[INSPIRE](#)].
- [61] Z. Ligeti, M. Papucci and D.J. Robinson, *New Physics in the Visible Final States of $B \rightarrow D^{(*)} \tau \nu$* , *JHEP* **01** (2017) 083 [[arXiv:1610.02045](#)] [[INSPIRE](#)].
- [62] M.A. Ivanov, J.G. Körner and C.-T. Tran, *Probing new physics in $\bar{B}^0 \rightarrow D^{(*)} \tau^- \bar{\nu}_\tau$ using the longitudinal, transverse, and normal polarization components of the tau lepton*, *Phys. Rev. D* **95** (2017) 036021 [[arXiv:1701.02937](#)] [[INSPIRE](#)].
- [63] M. Blanke et al., *Impact of polarization observables and $B_c \rightarrow \tau \nu$ on new physics explanations of the $b \rightarrow c \tau \nu$ anomaly*, *Phys. Rev. D* **99** (2019) 075006 [[arXiv:1811.09603](#)] [[INSPIRE](#)].
- [64] S. Bhattacharya, S. Nandi and S. Kumar Patra, *$b \rightarrow c \tau \nu$ Decays: a catalogue to compare, constrain, and correlate new physics effects*, *Eur. Phys. J. C* **79** (2019) 268 [[arXiv:1805.08222](#)] [[INSPIRE](#)].
- [65] P. Colangelo and F. De Fazio, *Scrutinizing $\bar{B} \rightarrow D^* (D\pi) \ell^- \bar{\nu}_\ell$ and $\bar{B} \rightarrow D^* (D\gamma) \ell^- \bar{\nu}_\ell$ in search of new physics footprints*, *JHEP* **06** (2018) 082 [[arXiv:1801.10468](#)] [[INSPIRE](#)].
- [66] R.-X. Shi et al., *Revisiting the new-physics interpretation of the $b \rightarrow c \tau \nu$ data*, *JHEP* **12** (2019) 065 [[arXiv:1905.08498](#)] [[INSPIRE](#)].
- [67] A.K. Alok, D. Kumar, S. Kumbhakar and S. Uma Sankar, *Solutions to $R_D-R_{D^*}$ in light of Belle 2019 data*, *Nucl. Phys. B* **953** (2020) 114957 [[arXiv:1903.10486](#)] [[INSPIRE](#)].
- [68] R. Mandal, C. Murgui, A. Peñuelas and A. Pich, *The role of right-handed neutrinos in $b \rightarrow c \tau \bar{\nu}$ anomalies*, *JHEP* **08** (2020) 022 [[arXiv:2004.06726](#)] [[INSPIRE](#)].
- [69] S. Kumbhakar, *Signatures of complex new physics in $b \rightarrow c \tau \bar{\nu}$ transitions*, *Nucl. Phys. B* **963** (2021) 115297 [[arXiv:2007.08132](#)] [[INSPIRE](#)].
- [70] S. Iguro and R. Watanabe, *Bayesian fit analysis to full distribution data of $\bar{B} \rightarrow D^{(*)} \ell \bar{\nu} : |V_{cb}|$ determination and new physics constraints*, *JHEP* **08** (2020) 006 [[arXiv:2004.10208](#)] [[INSPIRE](#)].
- [71] B. Bhattacharya, A. Datta, S. Kamali and D. London, *A measurable angular distribution for $\bar{B} \rightarrow D^* \tau^- \bar{\nu}_\tau$ decays*, *JHEP* **07** (2020) 194 [[arXiv:2005.03032](#)] [[INSPIRE](#)].
- [72] R. Dutta and A. Bhol, *$B_c \rightarrow (J/\psi, \eta_c) \tau \nu$ semileptonic decays within the standard model and beyond*, *Phys. Rev. D* **96** (2017) 076001 [[arXiv:1701.08598](#)] [[INSPIRE](#)].
- [73] LATTICE-HPQCD collaboration, *$R(J/\psi)$ and $B_c^- \rightarrow J/\psi \ell^- \bar{\nu}_\ell$ Lepton Flavor Universality Violating Observables from Lattice QCD*, *Phys. Rev. Lett.* **125** (2020) 222003 [[arXiv:2007.06956](#)] [[INSPIRE](#)].
- [74] R. Dutta, *$\Lambda_b \rightarrow (\Lambda_c, p) \tau \nu$ decays within standard model and beyond*, *Phys. Rev. D* **93** (2016) 054003 [[arXiv:1512.04034](#)] [[INSPIRE](#)].
- [75] S. Shivashankara, W. Wu and A. Datta, *$\Lambda_b \rightarrow \Lambda_c \tau \bar{\nu}_\tau$ Decay in the Standard Model and with New Physics*, *Phys. Rev. D* **91** (2015) 115003 [[arXiv:1502.07230](#)] [[INSPIRE](#)].
- [76] X.-Q. Li, Y.-D. Yang and X. Zhang, *$\Lambda_b \rightarrow \Lambda_c \tau \bar{\nu}_\tau$ decay in scalar and vector leptoquark scenarios*, *JHEP* **02** (2017) 068 [[arXiv:1611.01635](#)] [[INSPIRE](#)].
- [77] A. Datta, S. Kamali, S. Meinel and A. Rashed, *Phenomenology of $\Lambda_b \rightarrow \Lambda_c \tau \bar{\nu}_\tau$ using lattice QCD calculations*, *JHEP* **08** (2017) 131 [[arXiv:1702.02243](#)] [[INSPIRE](#)].
- [78] A. Ray, S. Sahoo and R. Mohanta, *Probing new physics in semileptonic Λ_b decays*, *Phys. Rev. D* **99** (2019) 015015 [[arXiv:1812.08314](#)] [[INSPIRE](#)].

- [79] T. Gutsche et al., *Analyzing lepton flavor universality in the decays $\Lambda_b \rightarrow \Lambda_c^{(*)}(\frac{1}{2}^{\pm}, \frac{3}{2}^{-}) + \ell \bar{\nu}_\ell$* , *Phys. Rev. D* **98** (2018) 053003 [[arXiv:1807.11300](#)] [[INSPIRE](#)].
- [80] F.U. Bernlochner, Z. Ligeti, D.J. Robinson and W.L. Sutcliffe, *Precise predictions for $\Lambda_b \rightarrow \Lambda_c$ semileptonic decays*, *Phys. Rev. D* **99** (2019) 055008 [[arXiv:1812.07593](#)] [[INSPIRE](#)].
- [81] E. Di Salvo, F. Fontanelli and Z.J. Ajaltouni, *Detailed Study of the Decay $\Lambda_b \rightarrow \Lambda_c \tau \bar{\nu}_\tau$* , *Int. J. Mod. Phys. A* **33** (2018) 1850169 [[arXiv:1804.05592](#)] [[INSPIRE](#)].
- [82] M. Blanke et al., *Addendum to “Impact of polarization observables and $B_c \rightarrow \tau \nu$ on new physics explanations of the $b \rightarrow c \tau \nu$ anomaly”*, [arXiv:1905.08253](#) [[DOI:10.1103/PhysRevD.100.035035](#)] [[INSPIRE](#)].
- [83] P. Böer, A. Kokulu, J.-N. Toelstede and D. van Dyk, *Angular Analysis of $\Lambda_b \rightarrow \Lambda_c(\rightarrow \Lambda \pi) \ell \bar{\nu}$* , *JHEP* **12** (2019) 082 [[arXiv:1907.12554](#)] [[INSPIRE](#)].
- [84] X.-L. Mu, Y. Li, Z.-T. Zou and B. Zhu, *Investigation of effects of new physics in $\Lambda_b \rightarrow \Lambda_c \tau \bar{\nu}_\tau$ decay*, *Phys. Rev. D* **100** (2019) 113004 [[arXiv:1909.10769](#)] [[INSPIRE](#)].
- [85] Q.-Y. Hu, X.-Q. Li, Y.-D. Yang and D.-H. Zheng, *The measurable angular distribution of $\Lambda_b^0 \rightarrow \Lambda_c^+ (\rightarrow \Lambda^0 \pi^+) \tau^- (\rightarrow \pi^- \nu_\tau) \bar{\nu}_\tau$ decay*, *JHEP* **02** (2021) 183 [[arXiv:2011.05912](#)] [[INSPIRE](#)].
- [86] N. Penalva, E. Hernández and J. Nieves, *Further tests of lepton flavour universality from the charged lepton energy distribution in $b \rightarrow c$ semileptonic decays: The case of $\Lambda_b \rightarrow \Lambda_c \ell \bar{\nu}_\ell$* , *Phys. Rev. D* **100** (2019) 113007 [[arXiv:1908.02328](#)] [[INSPIRE](#)].
- [87] F.U. Bernlochner, Z. Ligeti, M. Papucci and D.J. Robinson, *Interpreting LHCb’s $\Lambda_b \rightarrow \Lambda_c \tau \bar{\nu}$ measurement and puzzles in semileptonic Λ_b decays*, *Phys. Rev. D* **107** (2023) L011502 [[arXiv:2206.11282](#)] [[INSPIRE](#)].
- [88] A.K. Leibovich and I.W. Stewart, *Semileptonic Lambda(b) decay to excited Lambda(c) baryons at order Lambda(QCD) / m(Q)*, *Phys. Rev. D* **57** (1998) 5620 [[hep-ph/9711257](#)] [[INSPIRE](#)].
- [89] M. Papucci and D.J. Robinson, *Form factor counting and HQET matching for new physics in $\Lambda_b \rightarrow \Lambda_c^* \ell \nu$* , *Phys. Rev. D* **105** (2022) 016027 [[arXiv:2105.09330](#)] [[INSPIRE](#)].
- [90] M.-L. Du, E. Hernández and J. Nieves, *Is the $\Lambda_c(2625)^+$ the heavy quark spin symmetry partner of the $\Lambda_c(2595)^+$?*, *Phys. Rev. D* **106** (2022) 114020 [[arXiv:2207.02109](#)] [[INSPIRE](#)].
- [91] J. Nieves and R. Pavao, *Nature of the lowest-lying odd parity charmed baryon $\Lambda_c(2595)$ and $\Lambda_c(2625)$ resonances*, *Phys. Rev. D* **101** (2020) 014018 [[arXiv:1907.05747](#)] [[INSPIRE](#)].
- [92] P. Böer et al., *Testing lepton flavour universality in semileptonic $\Lambda_b \rightarrow \Lambda_c^*$ decays*, *JHEP* **06** (2018) 155 [[arXiv:1801.08367](#)] [[INSPIRE](#)].
- [93] J. Nieves, R. Pavao and S. Sakai, *Λ_b decays into $\Lambda_c^* \ell \bar{\nu}_\ell$ and $\Lambda_c^* \pi^-$ [$\Lambda_c^* = \Lambda_c(2595)$ and $\Lambda_c(2625)$] and heavy quark spin symmetry*, *Eur. Phys. J. C* **79** (2019) 417 [[arXiv:1903.11911](#)] [[INSPIRE](#)].
- [94] S. Meinel and G. Rendon, *$\Lambda_b \rightarrow \Lambda_c^*(2595, 2625) \ell^- \bar{\nu}_\ell$ form factors from lattice QCD*, *Phys. Rev. D* **103** (2021) 094516 [[arXiv:2103.08775](#)] [[INSPIRE](#)].
- [95] M.-L. Du, N. Penalva, E. Hernández and J. Nieves, *New physics effects on $\Lambda_b \rightarrow \Lambda_c^* \tau \nu^- \bar{\nu}_\tau$ decays*, *Phys. Rev. D* **106** (2022) 055039 [[arXiv:2207.10529](#)] [[INSPIRE](#)].
- [96] G. Martinelli, M. Naviglio, S. Simula and L. Vittorio, *$|V_{cb}|$, lepton flavor universality and $SU(3)_F$ symmetry breaking in $B_s \rightarrow D_s^{(*)} \ell \nu \ell$ decays through unitarity and lattice QCD*, *Phys. Rev. D* **106** (2022) 093002 [[arXiv:2204.05925](#)] [[INSPIRE](#)].
- [97] G. Martinelli, S. Simula and L. Vittorio, *Updates on the determination of $|V_{cb}|$, $R(D^*)$ and $|V_{ub}|/|V_{cb}|$* , [arXiv:2310.03680](#) [[INSPIRE](#)].